INFLAMMATION AND STEM CELL TRANSPLANTATION

by

Kenneth Lynn Urish

BS, The Pennsylvania State University, 2001

Submitted to the Graduate Faculty of

School of Engineering in partial fulfillment

of the requirements for the degree of

Doctor of Philosophy

University of Pittsburgh

2006

UNIVERSITY OF PITTSBURGH

SCHOOL OF ENGINEERING

This dissertation was presented

by

Kenneth Lynn Urish

It was defended on

August 24, 2006

and approved by

Bruno Péault, PhD, Professor, Pediatrics and Cell Biology and Physiology

Jon D. Piganelli, PhD, Assistant Professor, Pediatrics

Todd Przybycien, PhD, Professor, Bioengineering, Carnegie Mellon University

George Stetten, MD PhD, Associate Professor, Bioengineering

Dissertation Director: Johnny Huard, PhD, Professor, Orthopaedic Surgery, Molecular Genetics and Biochemistry, and Bioengineering

INFLAMMATION AND STEM CELL TRANSPLANTATION

Kenneth L. Urish, PhD

University of Pittsburgh, 2006

Myoblast transplantation has been investigated as a treatment for Duchenne Muscular Dystrophy and injured myocardial tissue. Multiple groups have isolated an early myogenic precursor population, termed muscle-derived stem cells (MDSCs) that have a superior ability to regenerate dystrophin-positive myofibers and improve cardiac function following an ischemic event as compared to more differentiated myoblasts. The initial local environment of these transplantations involves a high degree of inflammation and its associated major component, oxidative stress. Here, we report that a resistance to these stresses is an important factor determining the regenerative capacity of muscle stem cells in skeletal and cardiac muscle. MDSCs have an increased antioxidant capacity that protects them from intracellular oxidative damage while myoblasts have lower levels of survival and delayed differentiation following exposure to oxidative stress. These experiments were conducted using a series of high throughput assays that combine robotic live-cell microscopy with custom image analysis software. Further, when antioxidant levels in MDSCs are lowered to values comparable to myoblasts, the regenerative capacity of MDSCs decreases to levels comparable to myoblasts in both skeletal muscle and cardiac cell therapies. These findings indicate the important role inflammation plays in cell therapies, and identifies an important new mechanism by which stem cells display a unique regenerative capacity and also a new phenotype in selecting cell populations with enhanced regeneration capacity.

TABLE OF CONTENTS

LIST OF FIGURES

PREFACE

I owe a tremendous amount of gratitude to my dissertation advisor, Johnny Huard. These past three years have been a wonderful learning opportunity, and I have enjoyed them immensely. He has provided an outstanding training environment and mentoring. Merci.

This dissertation had two distinct projects: microscopy image analysis and the role oxidative stress in cell therapies. Each would have been impossible without the advice and encouragement of my dissertation committee including Bruno Péault, Jon D. Piganelli, Todd Przybycien, and George Stetten. I appreciate their time, expertise, and guidance.

Designing image analysis software to improve the quantification of images began as an idea, but would not be a reality without George Stetten's graduate class "Methods in Image Analysis". After one of the classes, a guest lecturer, Jonas August, spent three hours discussing an array of approaches to solve a particular technical problem. This conversation marked the beginning of a productive collaboration. Aaron Cois, the teaching assistant in the class, became a source of infinite knowledge on the many technical details of programming that saved me hours of debugging. Finally, the image analysis software would not have been written without the ITK toolkit and the dedicated community that has built it. Open source is open science.

The role of inflammation and oxidative stress in the regenerative capacity of muscle stem cells began from a series of scientific posters outside the laboratory of Jon Piganelli. He provided outstanding suggestions and advice that allowed the idea to mature and develop. While writing my NRSA proposal, the discussions with him and his associate, Clayton Matthews, were the source of shaping the application into a successful proposal. His patience and expertise has been invaluable.

The capstone of this work has been in the field of cardiac cell therapy. My success is built on the tireless effort and toil of the Cardiac Group in the Stem Cell Research Center: Sensei Masaho Okada, Sensei Thomas Payne, and Sensei Hideki Oshima. It has been a pleasure to work

with all of you. Arigatou. Further, I would like to gratefully acknowledge Kimimasa Tobita and Bradley Keller for their assistance with the cardiac functional analysis.

My training in the University of Pittsburgh Medical Scientist Training Program has been watched closely by my career advisor, Todd Przybycien. We only meet once a semester, but I always look forward to the long hike over to Carnegie Mellon to ground my thoughts. Further, I have had the fortunate opportunity to have my desk in the laboratory of Bruno Péault. He is an excellent scientist, and I have learned a great deal observing his creativity and scientific thought process.

Special thanks are owed to each member of the Stem Cell Research Center. The graduate students that have been my comrades in the lab, especially during the late nights, include: Greg Cooper, Karin Corsi, Mitra Lavasani, Wei Shen, and Jenny Zhou. A number of former graduate students that have blazed the trail: Dr. Tom Payne, Dr. Ron Jankowski, and especially to Dr. Bridget Deasy for always keeping her office door open. The final summer has been an intense experience, and the future MD/PhD Joe Vella finished a series of experiments and an inordinate amount of cell counting that allowed me to graduate. The laboratory has been fortunate to have an excellent technical staff (M. Branca, A. Lu, M. Huard, and J Tebbets) and administrative support staff (R. Sauder, J. Hollifman, and J. Cummins). Our laboratory manager, Burhan Gharaibeh was a source of a number of useful pieces of advice on my professional development and choice of laboratory footwear. To each and every visiting Japanese Fellows that has expanded my cultural horizons – Bokuwa tannaru gakusei desu, anatatachi ga bokuno sensei desu.

Two former mentors have built the foundation for my interests in research: Wayne Curtis and Bill Sayles. Dr. Curtis, my undergraduate honors thesis advisor, taught me the value of engineering in the biological sciences and the important role of loud music and washing dishes in the laboratory. His introduction to bioreactor design and mass transport launched the beginning of my professional interests. Mr. Sayles, my high school biology teacher, taught me the importance of good questions, the evils of pronouns, and the usefulness of intelligent but ignorant Martian friends. I still use these lessons on a regular basis. Have you thanked a green plant today? I have.

I would like to thank my parents and sisters for supporting and encouraging my pursuit of higher education. A PhD in engineering is a fair trade for being an officially licensed CPA in the state of Pennsylvania, New York, and Florida. Remember, nothing is bigger than e^{∞}.

Finally, I would like to acknowledge the financial support of the National Institute of Bioengineering and Biomedical Imaging at the National Institute of Health (1F31EB006292-01A). In particular, I owe a special acknowledgement to Richard Baird who has decided that the future training of an MD/PhD student is a valuable investment. This would not have been possible without Harvey Borovetz's support. Persistence is important. I have also had the fortunate opportunity to have the support of a number of industry relationships including Medtronic, Imaging Technologies at General Electric, and the people at Treestar that graciously donated a license to FlowJo, an expensive piece of flow cytometry analysis software.

The work presented here has been made possible by grants to Johnny Huard from the MDA, the NIH (R01-HL 069368-02), the Pittsburgh Tissue Engineering Initiative (PTEI), the Hirtzel Memorial Foundation, Jesse's Journey, and the Henry J. Mankin Chair. This investigation was conducted in a facility constructed with support from the NIH.

NOMENCLATURE

ANOVA, analysis of variance

carboxy-H_2DCFDA, 5-(and-6)-carboxy-2′,7′-dichlorodihydrofluorescein diacetate

CI, confidence interval

CNPase, 2',3'-cyclic nucleotide 3'-phosphohydrolase

DAPI, 4, 6'-diamidino-2-phenylindole

DEM, diethyl maleate

DMD, Duchenne muscular dystrophy

DMEM, Dulbecco's modified Eagle medium

EDA, end-diastolic area

EDD, end-diastolic dimensions

EP, early preplate, a population of myoblasts

ELISA, enzyme-linked immunosorbant assay

ESA, end-systolic area

ESD, end-systolic dimensions

FAC, fractional area change

FS, fractional shortening

GSH, reduced glutathione

GUI, graphical user interface

H_2O_2, hydrogen peroxide

ITK, the insight toolkit

LP, late preplate, a population of myogenic cells

LTP, long term proliferating cell, a population of MDSCs

LV, left ventricle

MCB, monochlorobimane,

MDSC, muscle-derived stem cell

NF-κB, nuclear factor kappa-B

PBS, phosphate-buffered saline

RI, regeneration index

ROS, reactive oxygen species

SOD, superoxide dismutase

STS, staurosporine

TNFα, tumor necrosis factor alpha

VEGF, vascular endothelial growth factor

vWF, von Willebrand factor

1.0 INTRODUCTION

Duchenne muscular dystrophy (DMD) is a debilitating disease characterized by the absence of dystrophin expression in the membrane-associated cytoskeleton of muscle fibers (Arahata et al., 1988; Bonilla et al., 1988; Hoffman et al., 1987; Miranda et al., 1988; Zubrzycka-Gaarn et al., 1988). Dystrophin is the essential link between the subsarcolemmal cytoskeleton and the extracellular matrix (Ervasti and Campbell, 1991; Ibraghimov-Beskrovnaya et al., 1992; Matsumura and Campbell, 1994; Matsumura et al., 1992; Ozawa et al., 1995), and disruption of this link results in muscle fiber necrosis and progressive skeletal muscle weakness (Bonilla et al., 1988; Menke and Jockusch, 1991; Watkins et al., 1988). Cell transplantation and a number of gene therapy modalities have been explored in an attempt to regenerate dystrophin-positive myofibers. This review focuses on the use of myoblasts for cell transplantation, including limitations of this technique such as poor cellular migration, immune rejection, and the inability of donor cells to survive a host's inflammatory response. Researchers working to surmount these initial limitations isolated postnatal muscle-derived stem cells (MDSCs), a population of early myogenic progenitor cells that exhibit a superior ability to regenerate dystrophic muscle. Various characteristics of these cells, including self renewal, long-term proliferation, multipotent differentiation, and immune-privileged behavior, lead to improved outcome after MDSC transplantation.

1.1 MYOBLAST TRANSPLANTATION

Initial animal studies revealed that injecting normal myoblasts (satellite cells cultured *in vitro*) into the muscle of *mdx* mice, a dystrophin-deficient animal model of DMD, regenerated dystrophin-positive myofibers to a limited degree. These simple results established two

important concepts. First, injected myoblasts can regenerate muscle fibers. Second, because dystrophin is only produced in multinucleated fibers, rarely in the injected mononuclear cells, these results confirmed the *de novo* synthesis of dystrophin in the normal location within the myofiber, the sarcolemma (Huard et al., 1991a; Huard et al., 1991b; Karpati et al., 1989; Partridge et al., 1989).

These initial promising results in *mdx* mice motivated researchers to launch a series of small-scale clinical trials testing the feasibility of myoblast transplantation (Gussoni et al., 1997; Gussoni et al., 1992; Huard et al., 1991a; Huard et al., 1992a; Law et al., 1990; Mendell et al., 1995; Tremblay et al., 1993). These studies revealed both short- and long-term dystrophin expression in the injected muscle, but the number of dystrophin-positive myofibers decreased after reaching a maximum one month after injection. These findings corresponded with initial observations of an apparent increase in muscle strength followed by a decrease back to baseline measurements.

1.2 INITIAL LIMITATIONS OF TRANSPLANTATION

Further investigations using the *mdx* mouse model revealed a number of obstacles inherent in myoblast transplantation. An observed specific immune response and nonspecific inflammatory response resulted in the survival of only a small fraction of the transplanted cells. Both of these problems are directly related to the initial oxidative stress induced inflammation and primary non-function. Complicating this problem was the limited migration of the injected myoblasts, which resulted in only a small, limited area of myofiber regeneration. These problems are outlined in Figure 1.

After cell transplantation, regenerating myofibers were visible only in areas in close proximity to the delivered cells, revealing limited migration of the myoblasts (Fan et al., 1996; Huard et al., 1994b; Morgan et al., 1993; Satoh et al., 1993). Muscle fibers are multinucleated; hundreds of nuclei extend along a single myofiber. After a donor myoblast fuses with a muscle fiber, dystrophin restoration does not extend beyond 310 μm of the nucleus, and in many cases the regeneration is unidirectional (Gussoni et al., 1997). Despite the poor migration of myoblasts

in *mdx* muscle, donor cell migration is even worse in normal, healthy muscle fibers (Smythe et al., 2000). Although some studies have shown that myoblasts can actively migrate to areas of injury in response to chemoattractants released from local macrophages (Bischoff, 1997; Grounds, 1996), transplanted myoblasts are unable to regenerate dystrophin-positive myofibers in areas other than those immediately surrounding the injection site. This limitation continues to impede the use of cellular therapy to treat DMD. However, inducing the expression of matrix metalloproteinases (MMPs) in myoblasts or injecting MMPs along with myoblasts significantly increases migration from the injection site (Caron et al., 1999; El Fahime et al., 2000; Ito et al., 1998; Torrente et al., 2000).

The most unsurprising obstacle encountered in myoblast transplantation is immune rejection of the transplanted cells. Compared to cell transplantation in immunodeficient mice, cell transplantation in major histocompatibility complex (MHC)-incompatible and tolerant host mice was less successful (Partridge et al., 1989). The use of immunohistocompatible donors and recipients for the first clinical trials still resulted in production of host antibodies in response to either donor myoblasts or myotubes (Huard et al., 1991a; Huard et al., 1992a; Torrente et al., 2001; Tremblay et al., 1993). Muscle biopsies revealed that lymphocytes surrounded the donor myoblasts (Gussoni et al., 1997). The immune response elicited by myoblast transplantation is intense. When used in an effort to improve the outcome of myoblast transplantation in mice and primates, the immunosuppressive agent cyclosporine A (Labrecque et al., 1992; Law et al., 1988) is less effective than Tacrolimus (FK506), a stronger immunosuppressive agent (Kinoshita et al., 1994; Lochmuller et al., 1996).

Subsequent work led to the characterization of two mechanisms that limit graft acceptance: a long-term specific immune response and an acute non-specific inflammatory response. These two processes may not be exclusive as early inflammatory events may trigger the immune system and limit graft acceptance. Transplanted donor myoblast are rejected even after delivery into immunohistocompatible mice. That finding suggests that dystrophin or an associated muscle protein acted as an antigen in the dystrophic mice. Although antibodies to dystrophin were identified in the host mice (Huard et al., 1992b; Ohtsuka et al., 1998; Tremblay et al., 1993), this particular immune response was not responsible for the long-term muscle fiber rejection (Bittner et al., 1994; Ferrer et al., 2000; Vilquin et al., 1995). Minor histocompatible antigens can induce graft rejection after allotransplantations in both humans and mice, and

researchers have posited that these minor antigenic differences may be responsible for the immune reaction observed after myoblast transplantation (Boulanger et al., 1997; Guerette et al., 1995; Huard et al., 1991a; Vilquin et al., 1995).

Initial studies of myoblast transplantation also identified an even more critical obstacle: A large majority of the injected cells were lost to a rapid inflammatory response that occurred immediately after injection (Beauchamp et al., 1994; Fan et al., 1996; Huard et al., 1994a). Later work revealed that less than 1% of the total number of injected cells remained within the recipient one month after transplantation (Beauchamp et al., 1999; Gussoni et al., 1992; Karpati et al., 1993; Mendell et al., 1995); Gussoni et al. (1997) reported that 3% to 14% of donor cells survived injection. A targeted immune rejection could not be responsible for this widespread cell death within such a short time span. Further, the cell death occurred even in the absence of a humoral immune response. The short-term reduction in the donor myoblast population was similar in immunodeficient, immunocompromised, and immunohistocompatible donors (Gussoni et al., 1997; Huard et al., 1994a). These factors suggest a more acute inflammatory response. Indeed, additional studies revealed infiltrating polymorphonuclear cells, macrophages, natural killer cells, and neutrophils surrounding the injected donor myoblasts. In addition, inhibiting the non-specific inflammatory response by using monoclonal antibodies that blocked leukocyte adhesion or by genetically engineering injected myoblasts to express anti-inflammatory interleukins improved initial myoblast survival (Guerette et al., 1997a; Qu et al., 1998). These results support the hypothesis of the non-specific inflammatory response; however, these gains cannot entirely account for the rapid cell loss that occurs after transplantation, which suggests that other events play an important but undefined role.

Perhaps the critical short-term factor responsible for successful myoblast transplantation does not hinge upon the immune response of the host but, rather, on the potential of the donor myoblasts. Normalization of the number of injected cells to exclude the cells eliminated during the first 24 hours after injection suggests that a small number of cells is responsible for the regeneration of a very large number of dystrophin-positive myofibers. Compared with the number of viable nuclei remaining after the enormous cell loss, the total number of donor nuclei within the resultant muscle grafts is dramatically higher (Beauchamp et al., 1999; Qu et al., 1998). Analysis of long-term myoblast transplantation grafts in human clinical trials showed that half of the donor myoblast nuclei had fused to host myofibers, and some of the donor myoblast

nuclei were found outside the sarcolemma closely associated with a single myofiber, similar to the location of satellite cells (Gussoni et al., 1997). These final two points suggest that the cells that survived after injection had a remarkable propensity for proliferation and differentiation.

Muscle development does not follow the simplistic model of a homogenous group of satellite cells fusing with myotubes to repair muscle fibers (Goldring et al., 2002; Seale and Rudnicki, 2000; Zammit and Beauchamp, 2001). Instead of transplanting a population of cells that would survive the initial inflammatory response and proliferate, researchers performing early studies of myoblast transplantation used a heterogenous population of efficient and inefficient cells, which decreased the potential for skeletal muscle regeneration. Was it possible to isolate this distinct population of muscle cells?

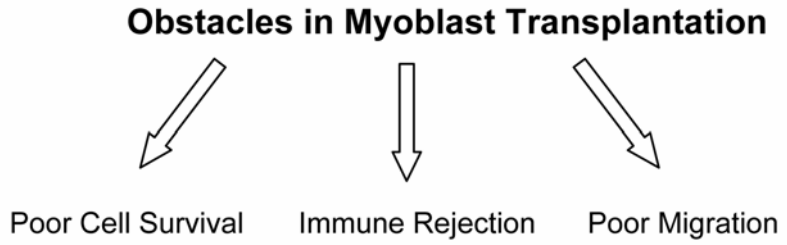

Figure 1: Obstacles in Myoblast Transplantation.
The three primary obstacles initially encountered in myoblast transplantation used to treat DMD patients

1.3 IMPROVED SKELETAL MUSCLE REGENERATION

Until recently, it was difficult to obtain pure skeletal myogenic cultures because primary cultures of disassociated muscle tissue contain an array of cell types. including neurovascular and connective tissue (Dai et al., 1992; Morgan et al., 1990; Partridge et al., 1989; Watt et al., 1982; Watt et al., 1984). Rando and Blau (Rando and Blau, 1994) developed a preplate technique that allows researchers to preferentially select myogenic cells and eliminate other non-myogenic tissue from the culture on the basis of the cell types' differing propensities to adhere to collagen-coated tissue culture flasks. Figure 2 illustrates the preplate technique (Richler and Yaffe, 1970).

If only a small minority of cells survived transplantation, researchers in our laboratory hypothesized that these cells were a special subpopulation of muscle cells (Qu et al., 1998). Furthermore, if the preplate technique could be used to separate myoblasts from non-myogenic cells, it also could enable the isolation of different populations of myogenic cells. Both of these hypotheses turned out to be correct.

The preplate technique can be used to isolate three distinct populations of myogenic cells discernable on the basis of their ability to regenerate dystrophic muscle. The population of cells isolated from the early preplate (EP) expressed myogenic markers, proliferation behavior, and regenerative capacity comparable to satellite cells. When cultured *in vitro*, EP cells divide a limited number of times before fusing and have a limited ability to regenerate dystrophin expressing myofibers *in vivo* (Qu-Petersen et al., 2002). The expression of an array of myogenic regulatory factors suggests that EP cells are strongly committed to the myogenic lineage (Jankowski et al., 2002a). The second population of skeletal muscle–derived cells, isolated from the sixth or subsequent preplates, was termed the late preplate (LP) cell population. These myogenic cells differ from the EP cells by exhibiting slower division and a lack of fusion with other myoblasts. LP cells can only be cultured for a limited time before they differentiate toward myofibers. However, after two weeks, clonal populations of a previously unidentified population appear from quiescent LP cells. This third myogenic cell population, termed long-term proliferating (LTP) cells, exhibits a superior ability to regenerate dystrophin-positive muscle fibers within *mdx* skeletal muscle when compared with satellite cells (Huard et al., 2003).

These LTP cells appeared to be an early progenitor population of myogenic cells on the basis of the cells' scarcity in muscle tissue and absence of the expression of myogenic genes, the most classic of these being MyoD. More importantly, muscle-derived cells from preplate 6 (PP 6) appeared to be the unique population of myoblasts that avoided rapid cell death after transplantation. When transplanted into skeletal muscle, cells from preplate 1 underwent rapid cell death, whereas most cells from preplate 6 survived after transplantation. Indeed, the PP 6 cells appeared to proliferate after injection (Qu et al., 1998; Qu and Huard, 2000) These experiments were completed in MHC-matched mice.

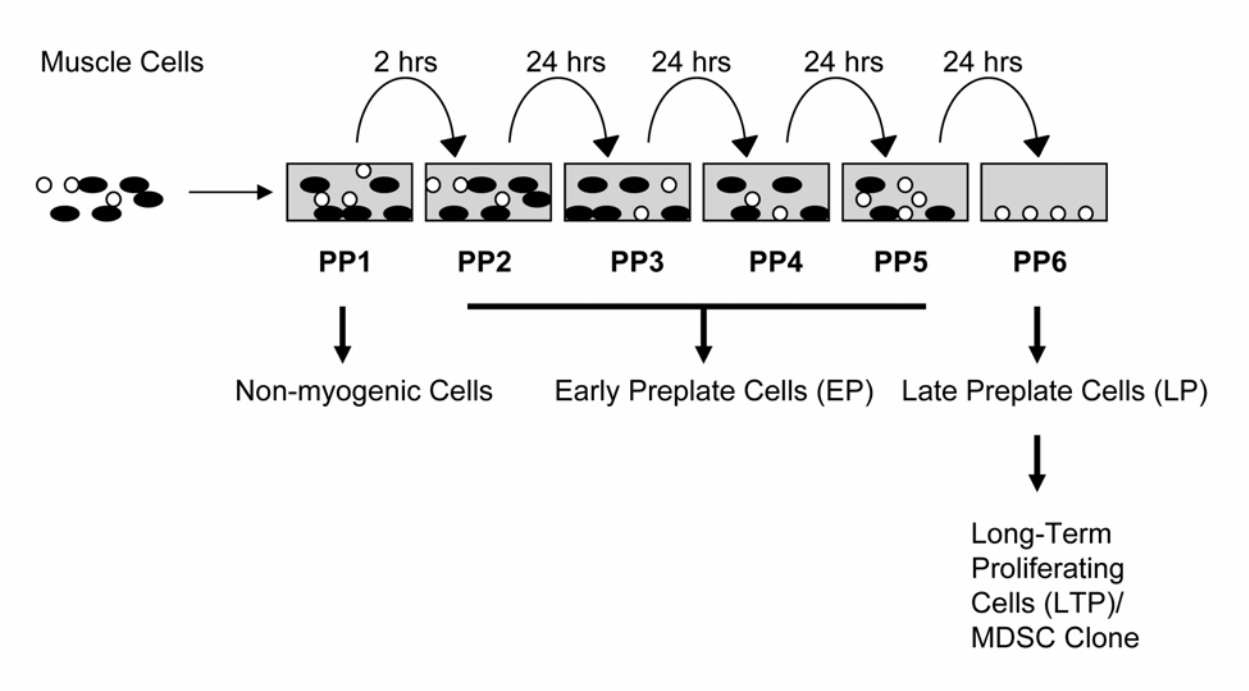

Figure 2: The preplate technique.
Dissociated skeletal muscle–derived cells harvested from a C57BL-6J and 10J mice are separated on the basis of their adhesion to collagen-coated flasks over a 4- to 7- day period. This technique leads to the isolation of three populations of cells distinguishable by their varied abilities to regenerate dystrophic muscle (Qu-Petersen et al., 2002). More than four different populations have been isolated by using the preplate technique followed by FACS for CD34, Sca-1, and c-kit (Jankowski et al., 2001).

1.4 MECHANISM OF IMPROVED MUSCLE REGENERATION

What was the mechanism behind the LTP cell population's increased ability to regenerate skeletal muscle? These early myogenic progenitor cells had a distinct phenotype that included relatively high levels of proliferation and a propensity for continued self-renewal. Furthermore, this cell population acted as a single unit capable of regenerating all the different cell types necessary for functional muscle. On the basis of their unique self-renewal properties and capacity to undergo multilineage differentiation, these LTP cells came to be called muscle-derived stem cells (MDSCs) (Deasy et al., 2003; Huard et al., 2003; Jankowski et al., 2002b).

Compared with satellite cells, MDSCs exhibit higher rates of proliferation and lower levels of fusion, which together lead to increased myofiber regeneration. After a progenitor cell fuses with a myotube, it loses the ability to proliferate and increase the number of dystrophin-positive myofibers in the dystrophic muscle. The bulk of satellite cells undergo a limited number of divisions before fusion (Jankowski et al., 2002a). These phenotypic characteristics are important across multiple animal models. Cell proliferation and differentiation correlate with skeletal muscle regeneration *in vivo* not only in mice after injection of mouse myogenic cells but also in rats after injection of rat myogenic cells (Jankowski and Huard, 2004). MDSCs have a CD34-positive phenotype that is associated with a superior ability to regenerate muscle fibers. Compared with CD34-negative LP cells, CD34-positive LP cells have a decreased tendency to fuse and exhibit higher levels of proliferation, despite the fact that both populations exhibit a similar low degree of myogenic commitment. Interestingly, as the cells begin to fuse they switch to a CD34-negative phenotype (Jankowski et al., 2002a).

The cellular division of MDSCs does not follow traditional exponential growth kinetics, which are based on the assumption that a cell population is 100% mitotically active. Similar to other stem cell populations, clonal populations of MDSCs exhibit the ability to self-renew. The cells follow non-exponential growth with various fractions of cells dividing or existing in different states of the cell cycle, including quiescence, at any given time. This asymmetric cell division is measurable *in vitro* (Deasy et al., 2001; Deasy et al., 2002). Mathematical analysis of the kinetics has revealed MDSCs to be a heterogeneous population of cells containing proportional numbers of cells that are quiescent, mitotically active, or differentiating (Deasy et al., 2003). This work was important because it established that MDSCs actively produce two populations of cells: a quiescent population for future muscle repair and a population of cells for immediate muscle repair. This behavior is similar to that of heterogeneous populations of muscle progenitor cells, which maintain distinct populations of quiescent and rapidly proliferating cells (Goldring et al., 2002; Zammit and Beauchamp, 2001).

Whereas their asymmetric division suggests MDSCs' capacity for self-renewal, *in vivo* studies have definitively demonstrated it. After MDSCs reconstituted the bone marrow of an irradiated mouse, bone marrow from that animal was able to rescue a second mouse; these results are indicative of a long-term repopulation capacity of MDSCs (Cao et al., 2003; Jackson et al., 1999). In addition, results demonstrating the multilineage potential of MDSCs (Lee et al., 2000;

Qu-Petersen et al., 2002) were generated from a single clonal cell. These experiments demonstrate that MDSCs possess the capacity for self-renewal after differentiation toward any of various tissue lineages. Such self-renewal is critical during muscle regeneration because it does not place a finite limit on the number of divisions that cells must undergo before differentiating toward myotubes.

The antigenic properties of a cell population also play a crucial role in the success of their engraftment. An initial clonal population of MDSCs induced a T-cell–mediated immune response similar to those observed in initial myoblast transplantation experiments. (Kimura et al., 2000; Qu et al., 1998). Another subclonal population, LTP cells, failed to elicit an immune response in immunocompetent mice and generated dystrophin-positive muscle fibers in grafts that persisted for more than 2 months (Fig. 3). These results support the findings of Qu-Petersen et al. (2002). Compared with myoblasts, LTP cells exhibit a superior ability to regenerate dystrophic skeletal muscle because injected LTP cells and the resultant dystrophin-positive myofibers are not destroyed by immune rejection. Interestingly, MDSCs have naturally low levels of MHC-I expression, a possible artifact of several passages *in vitro* (Qu-Petersen et al., 2002). Although MHC levels may hinder a T-cell–mediated immune response, a lack of MHC expression can activate an attack by natural killer (NK) cells (Vilches and Parham, 2002). Neural stem cells also exhibit low MHC expression and do not stimulate an NK or T-cell response. However, upregulating MHC expression on the neural stem cells by exposing them to interferon-gamma activates both NK and T-cells (Mammolenti et al., 2004). MHC-I expression can also be controlled by the intracellular redox balance. Inflammation can enhance and activate MHC-I expression on the cellular membrane. If MDSCs were more resistant to the initial inflammatory response, perhaps MHC-I expression was delayed or avoided. A great deal of work remains to define a plausible mechanism for the immune-privileged status of MDSCs.

The ability of MDSCs to regenerate muscle extends beyond the cells' capacity to generate a large number of myotubes that are not susceptible to immune rejection. The MDSCs also demonstrate pluripotency by regenerating not only myogenic cells but also the neurovascular cells that are necessary to completely regenerate the tissue. For example, an MDSC subclone expressed 2',3'-cyclic nucleotide 3'-phosphohydrolase (CNPase) and von Willebrand factor (vWF) markers *in vitro*, markers that are indicative of neural and endothelial cells, respectively. Stimulation of the clones with neuronal growth factor (NGF) and vascular

endothelial growth factor (VEGF) increased their expression of CNPase and vWF, respectively. In the cultures stimulated with VEGF, as the expression of vWF increased, the levels of desmin, an early marker of myogenic differentiation, decreased (Qu-Petersen et al., 2002). Nervous tissue and vasculature are essential to the survival of muscle tissue. The physical environment of regenerating muscle may induce MDSCs to differentiate into the multiple lineages necessary for complete muscle regeneration.

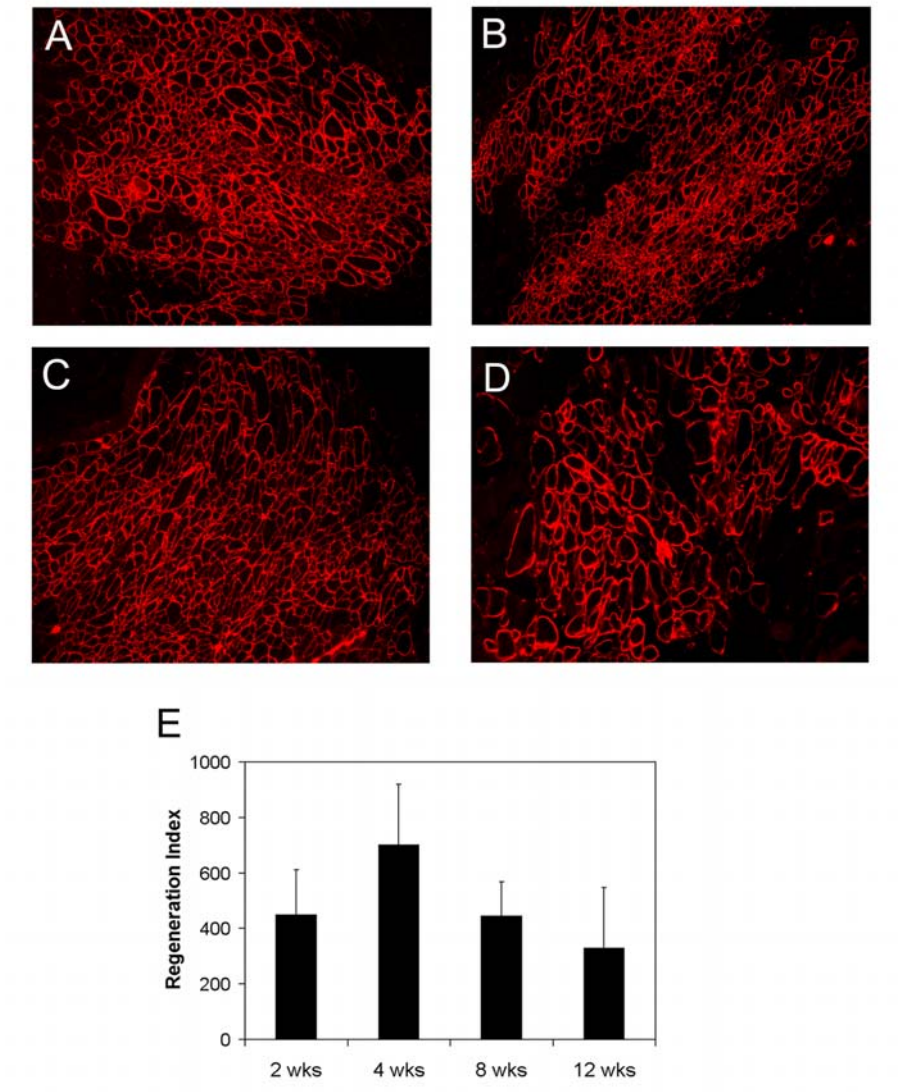

Figure 3: **MDSCs have an impressive ability to regenerate persistent dystrophin-positive myofibers in immunocompetent mice.**
A total of $2x10^5$ MDSCs were injected into both gastrocnemius muscles of 6-week-old *mdx* mice. The recipient mice were sacrificed at specific time points, and the muscle was immunostained for dystrophin. Typical results are shown 2 wks (A), 4 wks (B), and 8 wks after injection (C). All images are at 100x magnification. The dystrophin-positive myofibers were counted at each time point (n=4), and this number was presented as a function of the regeneration index: the number of dystrophin-positive myofibers normalized to $1x10^5$ injected cells (D). The regeneration index remained relatively constant between each time point (450±163 at 2 wks, 702±218 at 4 wks, and 446±121 at 8 wks). A two-tailed *t* test revealed no statistical difference between the regeneration indices calculated at each time point (2 vs. 4 wks, *P*=0.11; 2 vs. 8 wks, *P*=0.97; 4 vs. 8 wks, *P*=0.08). These results support the work of Qu-Petersen et al. (2002).

1.5 MDSCS AND THE DEVELOPMENT OF MUSCLE

Conventional thought in muscle regeneration included a model of quiescent satellite cells that were activated by muscle injury, proliferated into myoblasts, and fused to form myotubes. The small population of transplanted cells responsible for the majority of muscle regeneration and the isolation of adult MDSCs did not agree with this model. Instead, these findings added to a growing body of evidence suggesting that multiple, distinct populations of satellite cells reside in muscle and play different roles during regeneration (Goldring et al., 2002; Seale and Rudnicki, 2000; Zammit and Beauchamp, 2001).

At a minimum, satellite cells comprise two distinct cell populations: quiescent and highly proliferative cells. A picture of the two populations emerged as studies demonstrated the self-renewal ability of satellite cells (Zammit and Beauchamp, 2001). The identification of two distinct patterns of growth kinetics offered the first evidence that not all satellite cells are equivalent (Grounds and McGeachie, 1987; McGeachie and Grounds, 1987; Schultz, 1996). Other studies showed a population of satellite cells that normally existed in a quiescent state but could form the rapidly proliferating population of cells responsible for regenerating muscle (Baroffio et al., 1996; Molnar et al., 1996; Yoshida et al., 1998). These findings suggested that the quiescent population of cells is a progenitor of the population of rapidly proliferating satellite cells. Additional irradiation experiments supported the existence of this quiescent population. Initially, mononucleated cells failed to migrate from myofibers irradiated *in vitro*. However, at later time points, a second population of myogenic cells were observed to migrate off of the cultured myofiber suggesting that they were initially a quiescent population. (Gross and Morgan, 1999; Heslop et al., 2000; Quinlan et al., 1995; Wakeford et al., 1991). Connecting the expression of β-galactosidase to the expression of Myf5, the earliest marker of myogenic commitment, these two populations could be distinguished from each other by the expression of CD34 (Beauchamp et al., 2000).

Initially, researchers believed MDSCs to be one of these populations of satellite cells (Gussoni et al., 1999), but further investigation revealed that MDSCs were a more undifferentiated precursor of satellite cells. Satellite cells are defined by a combination of their morphologic location next to the muscle fiber and their expression of several cell markers and transcription factors outlined in Figure 4, including m-cadherin, desmin, and Pax7 (Zammit and Beauchamp, 2001). MDSCs are distinguishable from satellite cells on the basis of cell marker expression patterns; the ability of MDSCs to differentiate into multiple lineages, including blood;

and, importantly, the superior ability of MDSCs to regenerate dystrophin-positive myotubes (Deasy et al., 2001; Huard et al., 2003; Jankowski et al., 2002b).

The latter of these genes, Pax7, was initially regarded as a signal of MDSCs' commitment to the myogenic lineage because Pax7 knockout mice completely lack satellite cells but contain a normal size population of MDSCs (Seale et al., 2000). Further study revealed a more complicated picture. Other groups subsequently reported that Pax7 knockout mice actually do possess a satellite cell population as defined by morphologic location and CD34 expression. However, compared to normal mice, these mice contain a smaller population of satellite cells that are unable to completely repair injured muscle (Oustanina et al., 2004). A new picture is emerging in which Pax7 helps control satellite cell proliferation and self-renewal (Olguin and Olwin, 2004; Oustanina et al., 2004; Zammit et al., 2004). A schematic of a proposed model for the development of a myofiber appears in Figure 4.

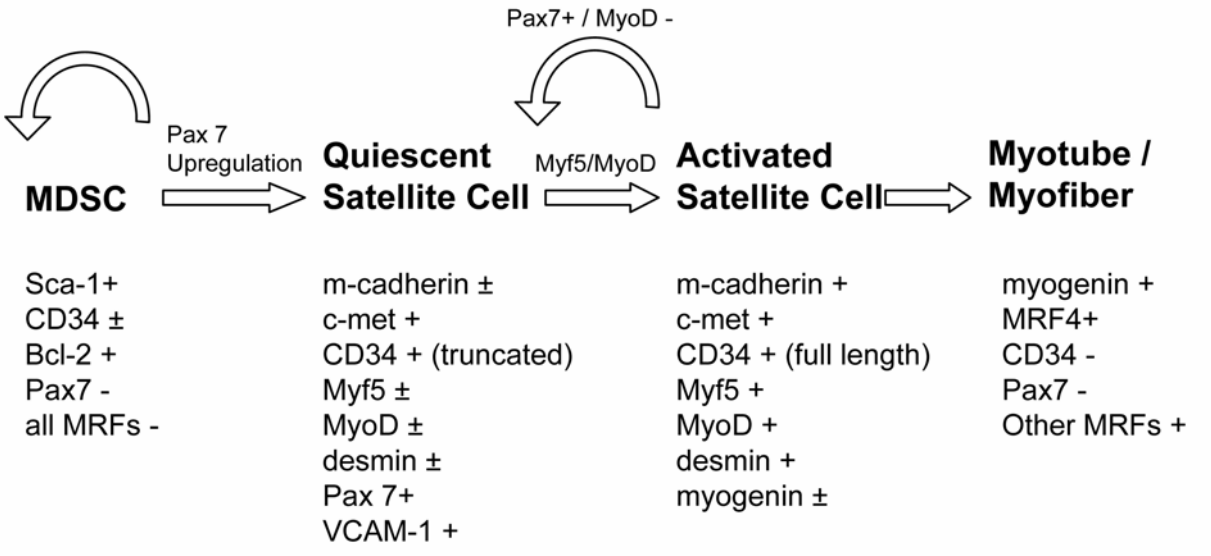

Figure 4: A possible mechanism of myogenic differentiation.
A possible mechanism of myogenic differentiation. Key cell marker differences between MDSCs and satellite cells include an upregulation of myogenic regulatory factors (MRF), including Pax7, c-Met, Myf5, and desmin. Cell markers used to distinguish the different stages of myogenic cells are based on the following references: (Beauchamp et al., 2000; Cornelison and Wold, 1997; Jackson et al., 1999; Lee et al., 2000; Qu-Petersen et al., 2002; Seale and Rudnicki, 2000; Seale et al., 2000; Yoshida et al., 1998; Zammit et al., 2004). Discrepancies are noted as ±.

1.6 TISSUE ENGINEERING AND MDSCS

The ability of the MDSCs to differentiate into various lineages in muscle tissue prompted our group to explore the ability of these cells to repair osteogenic defects. After being transduced with a vector to express bone morphogenetic protein 2 (BMP-2) and injected into the bone of an allogenic host, the cells formed bone matrix and differentiated into osteocytes and osteoblasts (Bosch et al., 2000; Lee et al., 2000; Musgrave et al., 2000; Shen et al., 2004a). When implanted in a critical-size skull defect in mice, these cells healed the bone defect (Lee et al., 2000; Shen et al., 2004a) Critical to the definition of a stem cell, when implanted in a large defect in a mouse femur, MDSCs underwent osteogenic differentiation and facilitated almost complete functional recovery. The repaired femur was similar to a normal uninjured femur in terms of strength and biomechanical properties (Shen et al., 2004b).

Muscle derived stem cells have also been shown to differentiate into hematopoietic lineages (Cao et al., 2003; Gussoni et al., 1999; Jackson et al., 1999). By using FACS Hoechst 33342 exclusion, it is possible to isolate from muscle tissue a population of stem cells, termed side population (SP) cells because they were a side population of the collected sample; these cells can regenerate dystrophin-positive myofibers in *mdx* mice and repopulate the bone marrow and rescue lethally irradiated mice (Gussoni et al., 1999). Cao et al. (2003)(Cao et al., 2003) demonstrated that MDSCs can differentiate toward hematopoietic lineages while, at least partially, preserving their myogenic potential. Bone marrow isolated from a primary mouse recipient could rescue a second irradiated mouse and regenerate dystrophin-positive myofibers in its muscle. This study demonstrated the ultimate level of plasticity of MDSCs; the cells changed their lineage in response to the local environment. These experiments also provide a classic, rigorous test of the multilineage differentiation potential of MDSCs by going beyond a simple evaluation of cell marker expression and assessing the ability of MDSCs to rescue irradiated mice, an assay that demonstrated the ability of MDSCs to differentiate into functional blood cells.

Stem cell–based therapy holds promise as a possible treatment for DMD, but there are still several hurdles to overcome before clinical applications become reality. First, after very extensive passaging *in vitro,* clonal populations of MDSCs develop a heterogeneity that limits their ability to regenerate muscle. Second, MDSCs are an exceptionally rare type of myogenic

cells, which means that a degree of expansion would be necessary to generate the quantities of cells required for any clinical therapy. Third, the immune acceptance of injected cells is critical, which means that the mechanism behind the unique immune-privileged status of certain myogenic populations needs to be better understood. Finally, the delivery method of the cells needs to be improved. Stem cells delivered intra-arterially have regenerated muscle and restored muscle function in α-sarcoglycan knockout mice (Sampaolesi et al., 2003). The expression of adhesion molecules can enhance the efficiency of systemic delivery of MDSCs by increasing their homing potential (Torrente et al., 2003). Systemic delivery is potentially advantageous in terms of safety, simplicity, and effectiveness and may provide a therapeutic benefit for treatment of DMD. Finally, additional study is needed to more fully evaluate the functional improvements elicited by myoblast transfer therapy.

On a technical note, a limitation in the field includes the inability to automate the quantification of the levels of regeneration and cell phenotypes *in vitro*. The first portion of this dissertation will focus on developing and improving these technologies. In the final section, these technologies will be utilized to investigate the mechanism behind the superior regenerative capacity of MDSCs as compared to myoblasts.

1.7 PROJECT OBJECTIVES

1.7.1 Objective #1: Development of Automatic Thresholding Algorithm

MDSCs have shown an enormous potential as a useful cell population in dystrophic skeletal muscle therapies. However, quantifying levels of dystrophin-positive myofiber regeneration is slow and time consuming. Further, accurate software does not exist primarily because of limitations in the development of efficient automatic threshold algorithms. We develop and validate an automatic threshold routine that can be useful in these tasks.

1.7.2 Objective #2: Robotic, Live-Cell Microscopy High Throughput Assays.

A series of survival and differentiation assays were needed to characterize phenotypic differences between myoblasts and MDSCs. Novel image analysis software was designed that automated a live cell microscopy technique, and created efficient, accurate, and high throughput assays that were critical to completing experiments discussed in objective #3. This is an interesting new technical approach to conducting live cell microscopy because analysis is conducted in a similar fashion to flow cytometry.

1.7.3 Objective #3: Mechanism of Increased Regenerative Capacity of Muscle Stem Cells: Role of Oxidative and Inflammatory Stress

MDSCs have a superior ability to regenerate dystrophic skeletal myofibers and improve the function of cardiac tissue following ischemic episodes as compared to myoblasts (EP cells). Previous work has demonstrated that MDSCs long term capacity for proliferation and multipotency may play an important role. However, many groups have observed inflammation at the site of myoblast transplantation in both skeletal and cardiac cell transplantation. We hypothesized that perhaps an important, unconsidered phenotype in MDSCs' regenerative capacity was a resistance to oxidative stress. We assessed the survival and differentiation phenotypic ability of MDSCs and myoblasts to resist oxidative and inflammatory stress. We then observed any differences in antioxidant capacity. Finally, we completed an extensive series of experiments to decrease levels of MDSCs' antioxidant capacity to similar levels as myoblasts. We assessed any differences in regeneration capacity of the MDSCs and MDSCs with decreased antioxidant capacity in the dystrophic skeletal muscle and ischemic cardiac animal models. Image analysis technologies served an important role in conducting these experiments.

2.0 UNSUPERVISED SEGMENTATION FOR MYOFIBER COUNTING

2.1 INTRODUCTION

Immunohistochemistry is a valuable technique that measures protein expression in cell culture and tissue sections by labeling a protein, such as dystrophin, with an antibody attached to a fluorescent signal. Many research groups are interested in automating the measurement of muscle regeneration in therapies for muscular dystrophy. The gold standard for measuring muscle regeneration uses immunohistochemistry to stain dystrophin-positive myofibers on a longitudinal muscle section so that the number of regenerated myofibers can be counted. Current therapies result in a few thousand myofibers being generated in a single muscle (Qu-Petersen et al., 2002). Manually counting such a large quantity is tedious and time consuming, but remains standard practice due to the lack of an accurate automated processes. Further, this analysis only assesses the local expression of dystrophin, but ignores the longitudinal distribution of dystrophin expression, i.e. the distribution of dystrophin expression as a function of position along the muscle fiber. This is one of the main limitations of current therapies (Urish et al., 2005). To design experiments that address this problem, we developed an algorithm to automatically count the number of dystrophin-positive myofibers on an immunofluorescent image, allowing three-dimensional dystrophin expression to be quantified.

2.2 UNSUPERVISED THRESHOLDING

Thresholding is often used to segment an image. Ideally, the two populations of pixels to be classified (foreground and background) would have distinct ranges of image intensities with minimal overlap to form a bimodal histogram (Fig. 5). However, images of myofibers

immunostained for dystrophin (Fig. 5B) and immunofluorescent images in general have unimodal image histograms (Fig. 5C) where an appropriate threshold is not obvious. We have developed an algorithm to automatically select a threshold for immunofluorescent images by searching for the threshold which maximizes the number of connected components of the thresholded image.

We have observed that the number of connected components as a function of threshold is smooth in the vicinity of the maximum. The search for this optimal threshold is implemented using a modified bisection method. Cells typically have a pixel area greater than 100 pixels (Retiga 1300 camera at 200x magnification) so that components below 50 pixels, the only input parameter, were ignored to eliminate noise. This approach is based on the following logic. If the threshold is set too low, the number of connected components is too low because some of the myofibers will not be detected (Fig. 6B). Conversely, if the threshold is too high, the number of connected components is too low because the white border separating the myofibers is eroded away connecting individual myofibers (Fig. 6D). This suggests that a reasonable threshold maximizes the number of sub-thresholded connected components (Fig. 6E). If this optimum threshold is used, from an anecdotal perspective, the image appears to be correctly segmented (Fig. 6C) compared to the original image (Fig. 6A). This algorithm is a variant of a method termed topological stable-state thresholding (Pikaz and Averbuch, 1996).

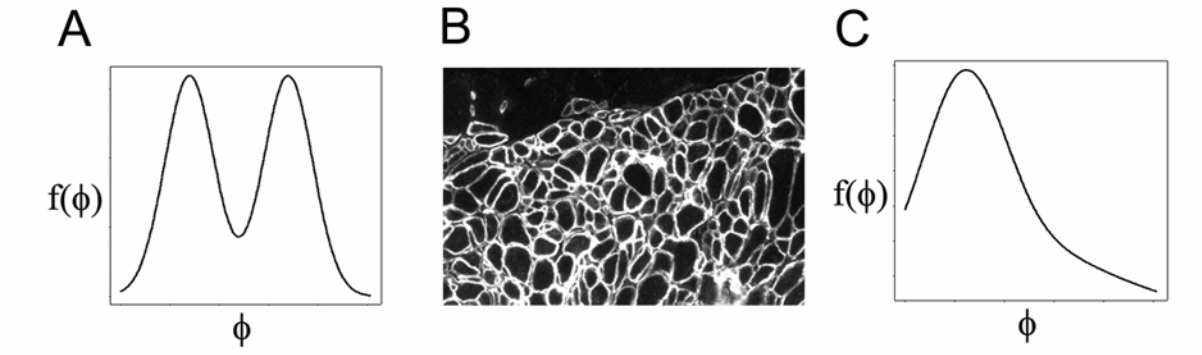

Figure 5: Possible Image Histograms.
The threshold used to separate two populations is apparent if the image histogram is bimodal (A). However, an immunofluorescent image of myotubes immunostained for dystrophin (B) has a unimodal image histogram (C), and the appropriate threshold is not clear. Note that (B) is only a small portion of the overall image of a regenerated muscle. Here, Φ represents pixel intensity.

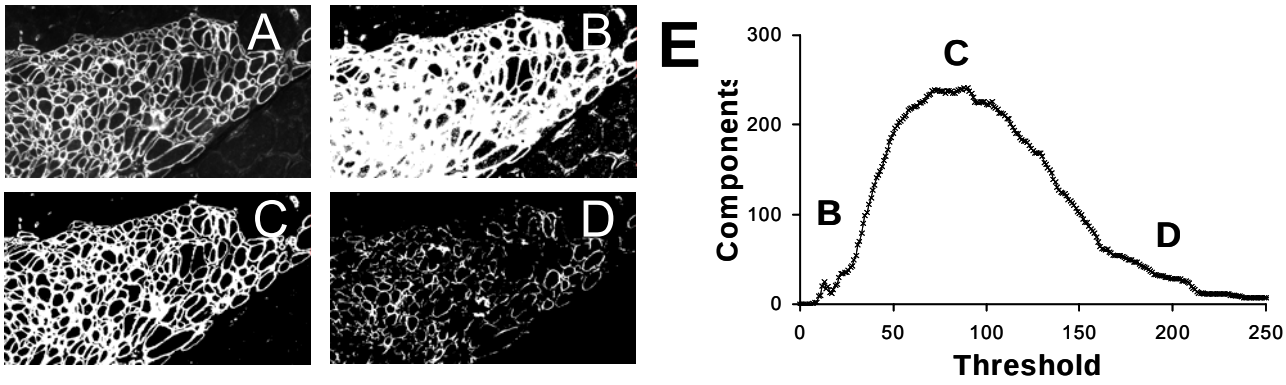

Figure 6: Outline of Stable State Thresholding Strategy.
The original image (A) is thresholded at a low (B), medium (C), and high (D) pixel intensity. The number of connected components above a user defined minimum area is plotted if the image was thresholded at all pixel intensities (E). Images B, C, and D are shown at their respective points on the curve in E. This suggests that an optimal threshold point can be identified based on maximizing the number of connected components in an image.

2.3 PROPOSED METHOD AND ITK IMPLEMENTATION

The Insight Toolkit (ITK) is an open source C++ library used to design and implement algorithms for image analysis (Yoo et al., 2002), and was used to rapidly assemble and test the feasibility of this method. Figure 7 outlines the pseudo-code of the algorithm using a modified bisection method. The minimum and maximum pixel intensities of the image are the set as the two endpoints. Each segment between an endpoint and the midpoint is bisected for the initial two evaluation points. The image is thresholded at each point, and the ITK classes, ConnectedComponentsImageFilter and RelabeledComponentsImageFilter, are used to count the

number of connected components above the minimum object size on each binary image. The point with the higher number of objects is set as the new midpoint, and the point with the lower number of objects is set as the new endpoint. The process is repeated until the two endpoints are two pixel intensities apart. Any number of other numerical methods for optimization without derivatives can be used to search for the maximum including Brent's and the golden ratio method.

This method of unsupervised segmentation has two inherent advantages. First, the only necessary input is the minimal area of the segmented objects; this parameter is known a priori, which we can exploit to help eliminate background noise. Second, the method employs a natural coarse-to-fine search strategy. Since the function is sampled at the three most widely separated intensities in the initial iteration, the function is, in effect, smoothed at a large scale and thus avoid local maximums. The sample selection has the effect of reducing the degree of smoothing with each iteration, i.e., decreasing as the search scale as the estimated maximum is approached. (We note that subsampling is a well-known strategy for regularizing ill-conditioned inverse problems, such as numerical differentiation.) It is possible that a local maximum near the global maximum may be identified; however this is an equally acceptable solution as little difference exists between the two answers in terms of number of components, which is the desired objective.

Further, ITK is a valuable tool to implement automated threshold-based segmentation of immunofluorescent images. Different numerical methods or other approaches can easily be tested to identify the best optimization or search strategy. The generic ITK pipeline allows the easy addition of edge enhancement features in situations where thresholding is not an entirely sufficient method for segmentation. In addition, standard image processing operations such as connected components that are challenging to code and debug are already reliably implemented in ITK.

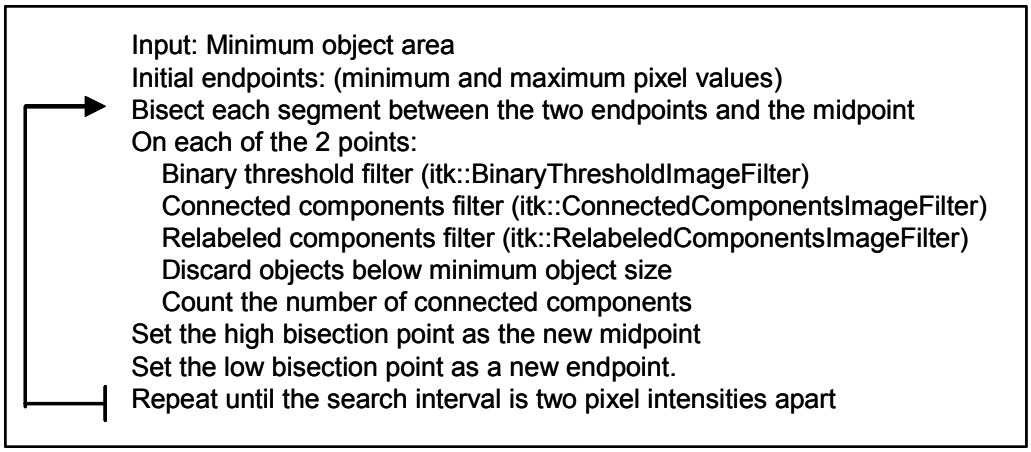

Figure 7: Outline of Topological Stable State Thresholding Algorithm.
The proposed method for unsupervised segmentation of immunofluorescent myofiber images uses a modified bisection method to search for the threshold point.

2.4 RESULTS AND DISCUSSION

To test the ability of this approach to measure three-dimensional regeneration, a series of serial cryostat sections of a regenerated muscle was stained, imaged, and measured with our algorithm. A longitudinal plot of the number of dystrophin-positive myofibers as a function of the length of the muscle, starting at the beginning of the engraftment, demonstrates the three-dimensional measurement of tissue regeneration (Fig. 8B). It was interesting to compare this method to other previously described and commonly used automatic threshold routines including the Otsu and Isodata methods (Otsu, 1979). As shown in Figure 9, both of these algorithms were extremely accurate when an image had a low number of objects, but had increasing levels of error as the number of objects in an image increased. The reverse was true with the topological stable state method. A major obstacle in therapies for muscular dystrophy is the low migration of dystrophin gene vectors that result in a limited longitudinal distribution of dystrophin expression (Urish et al., 2005). This automated algorithm will facilitate quantifying this measurement, allowing us to design experiments that address the limited distribution of dystrophin-positive myofibers.

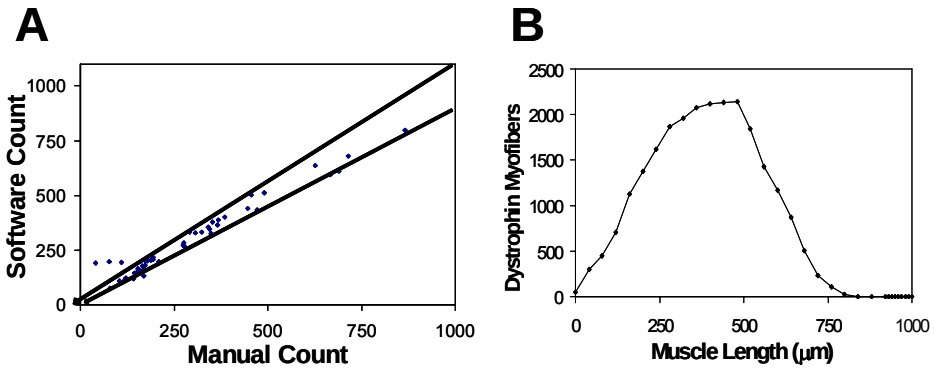

Figure 8: Validation of Topological Stable State Algorithm.
Validation of this algorithm (n=63) revealed that images that contained more than 100 objects varied by less than ±10% (solid lines) from manual counts (A). After validation, this algorithm was used to measure the number of dystrophin-positive myofibers on a set of 30 serial cryostat cross sections of a single muscle, and a longitudinal plot of the counts displays the 3-D distribution of dystrophin expression (B).

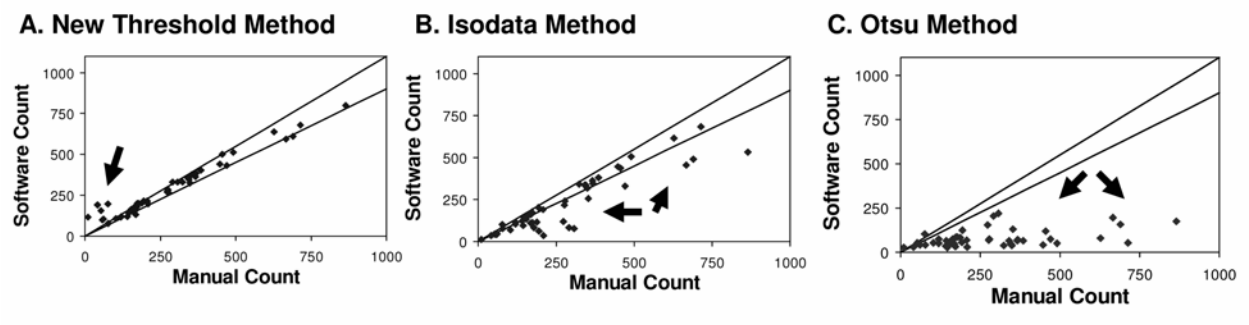

Figure 9: Comparison of Topological Stable State Thresholding Approach to other Methods
The number of dystrophin-positive myofibers on a series of 75 images was counted using A) the new automatic threshold method we have developed, B) the isodata automatic threshold method, and C) the Otsu automatic threshold method. Each point in the three plots is the separate image where the software count was compared to a manual count of myofibers. The lines are ± 10% disagreement between the software and manual counts. The arrows in each plot point out the regions where the software has more than 10% disagreement with the manual counts of the images, the gold standard of measurement. As shown, our method is very accurate when there are more than 100 myofibers in an image. This is the same point where the other two methods typically used in commercial software become error prone. The images we want to count have a large number of dystrophin-positive myofibers.

3.0 REAL TIME FLOW CYTOMETRY CONDUCTED USING ROBOTIC LIVE CELL MICROSCOPY

3.1 INTRODUCTION

Automated high-throughput microscopy has been used to describe cell phenotype including motility (Bahnson et al., 2005), proteomics (Perlman et al., 2004; Sigal et al., 2006), and genomic data (Neumann et al., 2006). Major technical hurdles in using automated microscopy for profiling strategies include image segmentation, analysis, and visualization of the results. Here we present imaging software that approaches high through-put microscopy from the perspective of flow cytometry. As a proof of concept, we have used the early apoptotic marker, annexin-V, to monitor levels of cell death over a continuous time period to validate the software and approach.

Flow cytometry and fluorescent microscopy have become essential techniques in the laboratory allowing different aspects of the cell to be observed and measured. In each case, there are three approaches to fluorescently label a cell: an antibody specific for a protein conformation tagged with a fluorescent molecule, a chemical that covalently binds with a macromolecule or becomes trapped in a cell, and fluorescent protein whose expression is linked to a particular transcription promoter. The last two types are particularly convenient in live cell microscopy because cells can be labeled and classified while they are still viable, and the state of the cell can be observed in response to stimuli or changes in environment. Flow cytometry is a valuable technique because of its powerful ability to rapidly quantify the light scattering and fluorescent properties of a cell, and then sort these populations for isolated, continued analysis *in vitro* or *in vivo*. Due to the automated nature, flow cytometry is particularly useful in quantifying a cell population due to its large sample size and cell specific measurements. However, detaching a cell from the culture flask may alter its state. Further, one sample can only be measured at one time

point. Fluorescent live-cell microscopy is valuable because it permits the observation of a cell for a prolonged time period while the cell is viable, and also possesses the quantitative potential that flow cytometry does.

Here, we propose combining the advantages of both live cell fluorescence microscopy and flow cytometry. A robotic stage microscope fitted with an incubator is used to image a series of locations on a cover-slip or culture plate at a repetitive time interval. Custom built, open source image analysis software is used to quantify the collected results. This allows full automated, unbiased observation and measurement of cell fluorescence. Cells are segmented on images using a loading dye and fractions of cells positive for a fluorescent signal and the strength of the signal are measured. The image analysis software sends output directly to a text file. Data is also written to a flow cytometry standard (FCS) file format (Seamer et al., 1997). This permits visualization and analysis using flow cytometry analysis software from a variety of vendors. The software developed in this study is freely available, and the source code can be downloaded and compiled on multiple platforms including, windows, macintosh, and linux operating systems.

3.2 RESULTS

3.2.1 Live Cell Microscopy is Similar to Flow Cytometry

The large number of images collected using robotic time-lapse fluorescent microscopy requires the use of automated image analysis software. Here, we used flow cytometry as a model in the analysis and presentation and design of our image analysis program. Initial steps in flow cytometry involve establishing acceptable gates to classify events as either noise or cells. In flow cytometry, this is accomplished gating the forward and side scatter events. Through observation we found that observing the histogram of the size of (PE/red) objects provided a reasonable means to distinguish noise and cellular objects. A second important concept in flow cytometry involves using controls to determine levels of background fluorescence and non-specific binding. Similar to flow cytometry, unstained controls were used to identify a threshold set point (Fig. 10). Threshold levels were selected on the basis of the point were FITC (green) objects became rare events on unstained control samples. Inaccurate threshold set points reveal obvious

distortions and noise. Events collected on each image were stored as events on FCS files for flow cytometry analysis. Fluorescent intensity was represented as the sum of the positive pixels in the image. Similar to adjusting the voltage and gain, each positive annexin pixel was multiplied by a constant factor to increase its intensity by an order of magnitude to ease visualization of FCS output plots. A typical sample size used in flow cytometry contains 5,000 to 10,000 events. However, flow cytometry has the capacity to measure a few thousand rare events in a sample of a few million cells. A single well imaged at 9 different locations over a 24hr period at 50-75% confluency would generate approximately 30,000 to 40,000 cellular events, resulting in the collection of 1,500 events an hour, similar to the normal sampling size of flow cytometry. Unlike the large sampling ability of flow cytometry, live-cell microscopy can easily monitor extremely low numbers of cells, a useful application in stem cell biology where populations of only a few hundred cells can be obtained.

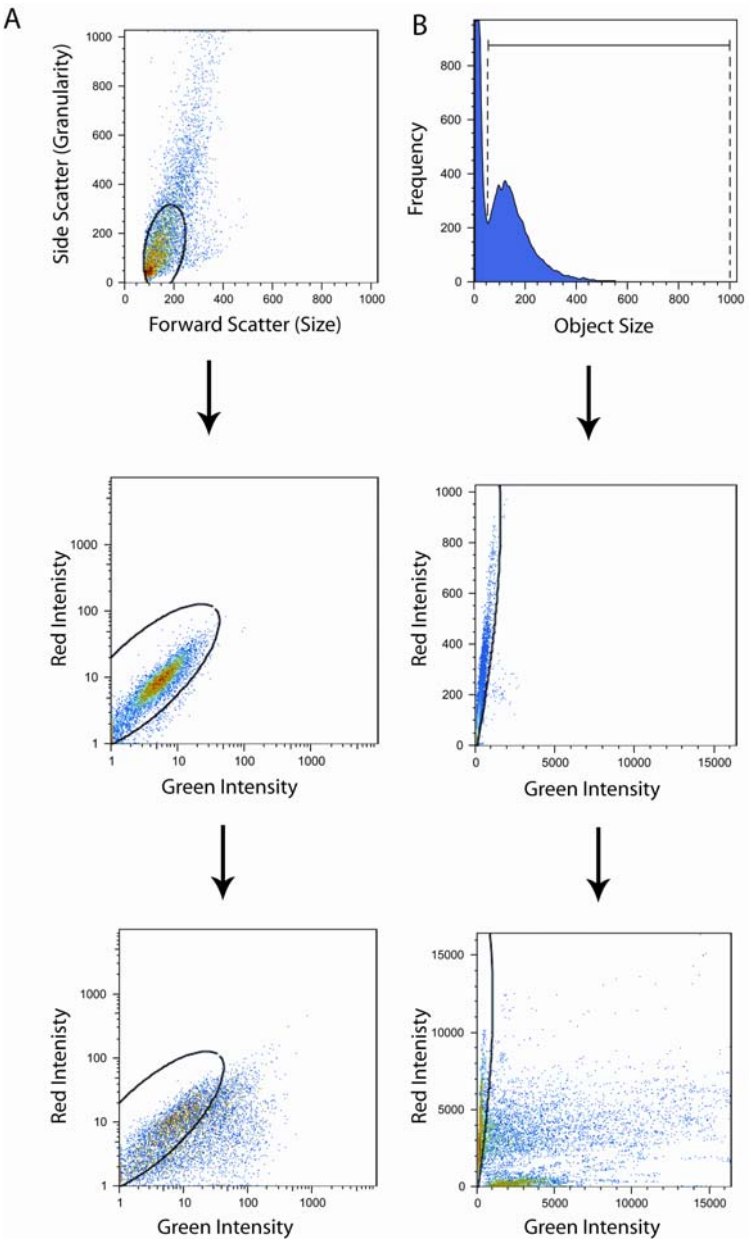

Figure 10: Work Flow Comparison between Flow Cytometry and Live Cell Microscopy
A work flow comparison between flow cytometry and robotic time-lapse fluorescent microscopy images analyzed using similar concepts as flow cytometry. (A) In flow cytometry, first cellular events are differentiated from noise based on light scattering properties (forward and side scatter) that indicate cell morphological properties. Second, background fluorescence levels are determined using unstained control samples. This allows a gate to be established to measure the fraction of the population positive for a fluorescent signal. (B) We designed automated image analysis software that takes thousands of microscopy images, segments the objects, and writes each object found on an image as a flow cytometry event on a flow cytometry file. Noise is differentiated from cellular events based on the size of the objects. Background fluorescence levels are determined using unstained control samples. This allows the fraction of the population positive for a fluorescent signal to be measured.

3.2.2 Development of Image Analysis Software

Robotic microscopy can generate tens of thousands of images in one data set. To facilitate the image analysis, quantification, and classification of such an enormous number of images, automated image analysis software was written using ITK, a C++ image segmentation and registration code library. Further to visualize the large number of images, output was written to a FCS file format for analysis using flow cytometry software. The program consists of three separate parts: The GUI interface, the image processing using ITK, and the C++ program to send all output as flow cytometry events to an FCS file format. Image inputs are handled through a batch-processing mode. The process is fully automated, and the image analysis parameters can be manually adjusted for increased accuracy including the parameters in background illumination and object recognition. Output is sent to a tab-delineated text file for data analysis using statistical packages and to an FCS file format for analysis with flow cytometry software.

The image processing is divided into three phrases: the preprocessing, segmentation, and analysis of the image. The image is acquired across three channels: PE and FITC fluorescence and the light microscopy image. Background illumination on both fluorescent images is removed by subtracting a gaussian blur of the respective image. To maximize the sensitivity of detecting solid objects, noise or cellular, in the PE channel, an automatic threshold algorithm, the Otsu method, is used to select a dynamic threshold set point (Otsu, 1979). After segmentation, each object is uniquely labeled using a 4-way connected components filter. In the FITC fluorescence channel, an alternative method was used to process the images collected from the FITC fluorescent channel to preserve the image intensities to allow for comparison. After the removal of background illumination, no further preprocessing was conducted to preserve original pixel intensities. Segmentation of objects in the FITC fluorescent channel was conducted using a standard binary threshold filter where the threshold set point was determined as based on unstained controls.

After segmentation, each FITC and PE object was assigned a unique label using a connected components algorithm, and each object was assessed for a number of different parameters including size, the sum of the pixel intensity, and average pixel intensity of the object. The fluorescent intensity of an object was defined as the sum of pixel intensities for the object. No image processing is applied directly to the light microscopy image, but segmentation

results from each of the fluorescent channels are overlaid onto the image to provide a visual validation of the accuracy of the analysis (Fig. 10). An important feature of the software is the inclusion and distinction between objects classified as either noise or objects. Objects considered cells are highlighted with PE pixels while noise is displayed with blue pixels. These can be viewed in the supplementary video #1 collected in the example discussed below.

3.2.3 Proof of Concept – Monitoring Levels of Cell Death

To test the performance of our software and its comparability to flow cytometry, we exposed a primary cell line, myoblasts, to increasing doses of staurosporine (STS) to induce apoptosis and cell death. Annexin-V, an early marker of apoptosis, was used to monitor cell death at 6 hour time intervals using flow cytometry and on a continual basis using robotic, live cell microscopy. Although our methods collects data over a continuous time period, it is impossible to validate this method at each time point using flow cytometry. Instead, 6 hour time intervals were selected for comparison between the two methods. Example dot plots at 6 hour time intervals over a 24 hour period are displayed in Fig. 11A and 11B. At each time point, it is possible to observe the evolution of a large population of annexin-(+) cells. These results are supported by a series of representative annotated output images from these respective time points (Fig. 11C).

Flow cytometry is a powerful method because of its quantitative ability. Results collected using both methods at each 6 hour time point were comparable (Fig. 12). Levels of annexin-(+) cells were comparable at low doses of STS, however at the higher doses the fraction of annexin-(+) cells were consistently higher using flow cytometry. This method involves a substantial number of sample manipulations, including harvesting the cells and multiple washes, prior to measurement which may increase the damage on an already fragile cell inadvertently increasing the fraction of the population positive for annexin-FITC. Cells were harvested using a gentle, dilute trypsin wash. Levels of apoptosis were not increased as compared if other harvesting approaches were used including gentle washes with EDTA solution.

An added benefit of conducting these measurements continuously is the ability to observe the continual progression of annexin-(+) cells. The quantified results from the direct analysis using the FCS formatted files of the live-cell microscopy are shown over time in the supplementary video #1. In this example, the morphological changes of the cell can be viewed

along with fluorescent intensity changes in each of the input screens while the processed output image displays the classification of each of the observed objects. Quantified results show a dose response, however the kinetic response at each dose can be seen (Fig. 12). Looking at individual time points, 500 and 5000nM STS appeared to have similar levels of cell death (Fig. 12C and 12D); however the continuous time plot of these doses reveals a trend (Fig. 12E). At 5000nM, the cell population had a faster response to STS and maintain a continuously higher fraction of annexin-(+) cell fractions. Observing the evolution of annexin-(+) cells over a continuous period of time allows trends to be distinguished from noise.

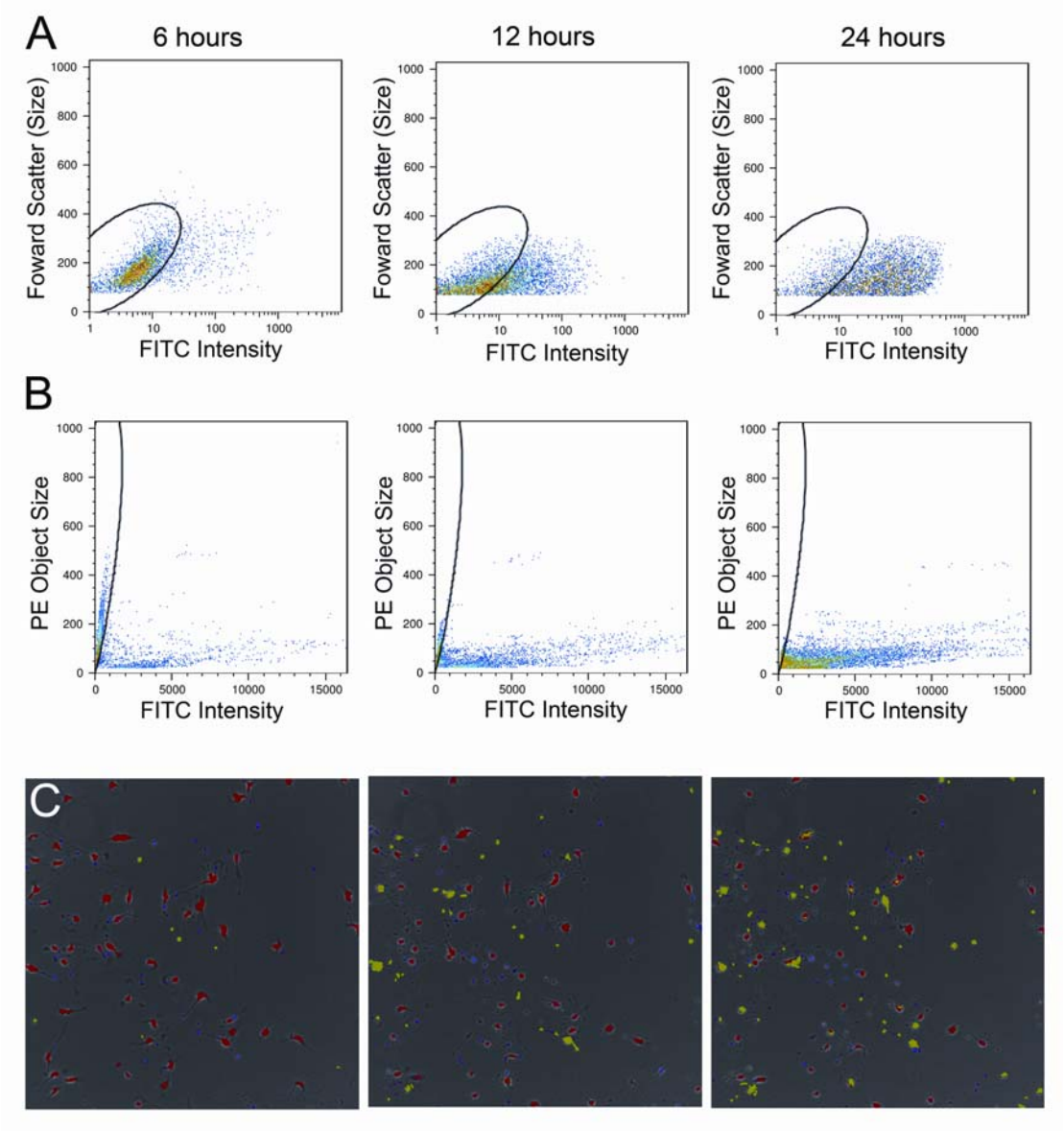

Figure 11: Comparison of Flow Cytometry and Live Cell Microscopy Output
A comparison of output FCS files between flow cytometry and our image analysis software. To validate the accuracy of this method, primary satellite cells were exposed to increasing doses of staurosporine (STS; 0 to 5000 nM) to induce apoptosis as measured by annexin-V FITC expression. (A) Flow cytometry dot plots are shown for each time point. (B) After the image analysis, the counted microscopy results are displayed as flow cytometry dot plots at selected time points of 6, 12, and 24 hrs. (C) Representative output images at 6, 12, and 18hrs of each processed image are annotated denoting cells (PE objects), apoptotic cells (FITC objects), and noise (blue and purple objects). Blue objects represent cellular noise and purple objects represent annexin-(+) object noise.

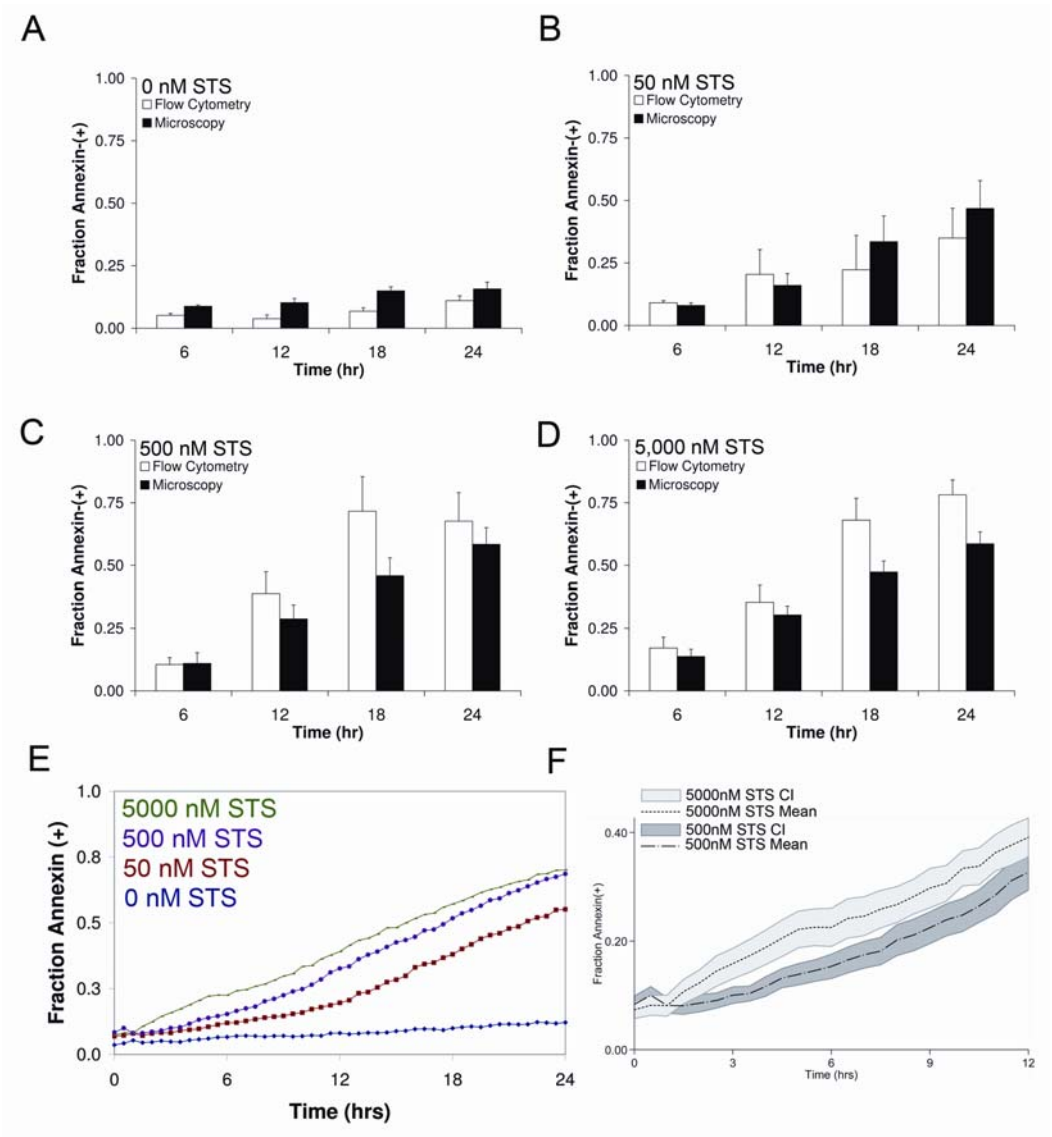

Figure 12: Comparison of Flow Cytometry and Live Cell Microscopy Apoptosis Fractions. Time course comparison of annexin-(+) cell fractions between flow cytometry and the image analysis software at increasing doses of STS. (A) At 0 nM STS, measurements collected using fluorescence microscopy had a trend of higher levels of cell death, but these differences were not significant. (B) Both methods had comparable annexin-(+) cell fractions at 50nm STS. Fractions of annexin-(+) cells at 500 and 5000nM STS were higher in the flow cytometry (C and D, respectively). These differences were significant at later time periods (P<0.05). The only significant differences in measurements at all doses and time points compared occurred in the final two 6 hour time points at the two highest doses. (E) The time plot of annexin-(+) cell fractions at each point at increasing doses of STS. The cell death profile of each dose contains 48 data points with 27 separate measurements. The confidence intervals are omitted to increase clarity. (F) The two highest doses of STS are highlighted during the early time period to demonstrate the ability to distinguish noise from trends. The shaded areas represent the confidence interval (CI) at each dose.

3.2.4 Photostability and Validation

In fluorescence microscopy, prolonged excitation and photoxidation can lead to a decrease in fluorescent signal. Next we explored if this loss in fluorescent signal prevented accurate cell tracking in both fluorescent channels over extended time periods. Cells loaded with tracking dyes experience a natural loss in fluorescent signal due to the diffusion of dye from the cell and from cell division. This loss in fluorescence signal can be observed in the representative histograms of average pixel intensity of PE objects at the initial 6 hour and final 24 hour periods. These histograms were collected from the control groups with no addition of STS and low levels of cell death, representing an actively dividing cell population (Fig 13D and E). Box and whisker plots used in Figure 13C provided a representation of the dynamic range of fluorescent intensity. The fluorescent shift of the entire group occurs in the initial 12 hours.

To verify that the annexin-V signal did not decrease over time we observed the changes in pixel intensity in the dose with the largest annexin-(+) populations in the myoblasts exposed to 500 and 5000 nM STS. The pixel intensity of objects identified as annexin-positive were observed over a prolonged time period and revealed no decrease in intensity (Fig. 13A and 13B). The histogram of the average pixel intensity of FITC objects at the initial 6 hrs and final 24 hrs revealed that little change occurred in fluorescent intensity. Further, the medians of these populations were not significantly different (P=0.56).

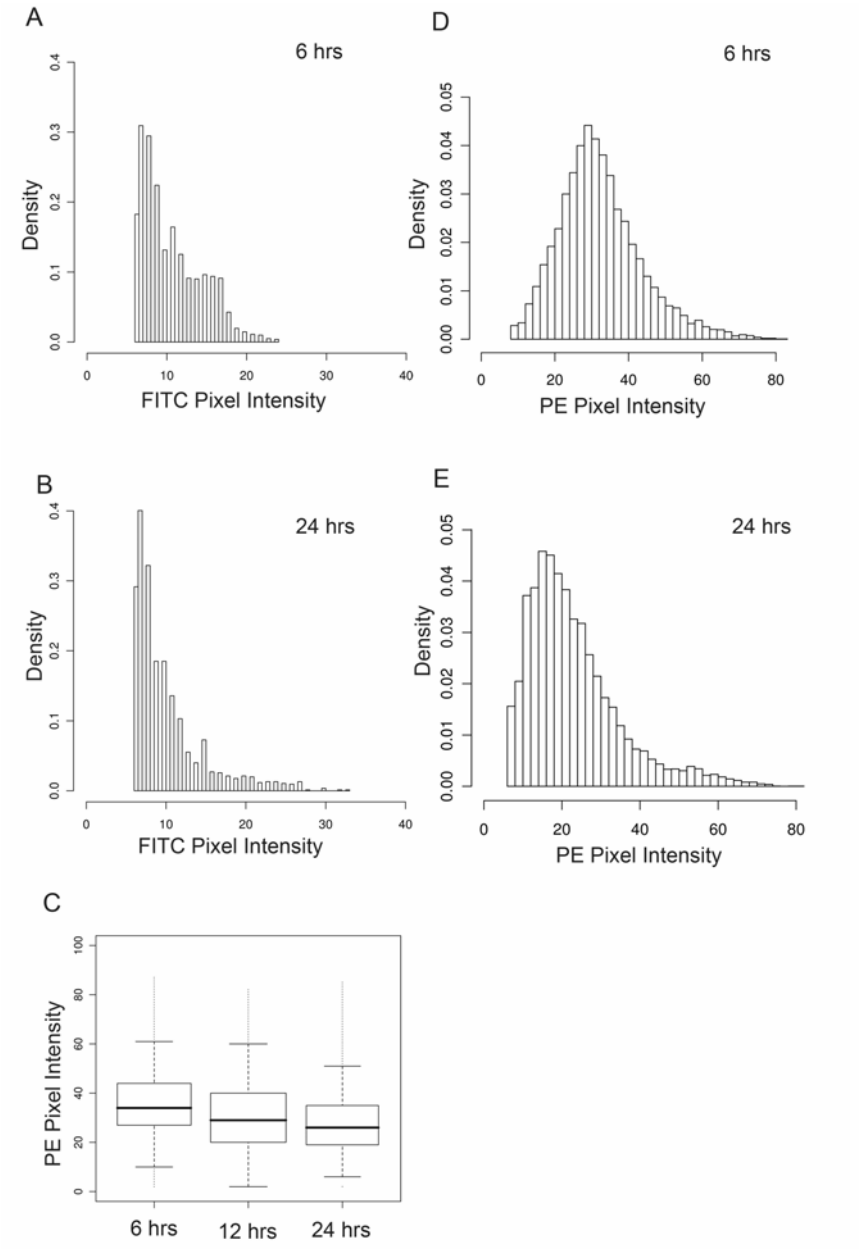

Figure 13: Photostability and Phototoxicity Concerns
Both fluorescent dyes maintain the necessary signal strength to be measured. Histograms of the average FITC object pixel intensity at 6 hrs (A) and 24hrs (B) reveal no change in intensity across 24 hrs. The medians of the average FITC pixel intensity are not significantly different. (C) The medians of the average PE pixel intensity are not significantly different, but a box and whisker plot reveals an observable shift in intensity. Histograms of the average PE object at 6 hrs (D) and 24 hrs (E) pixel intensity also show this shift.

3.3 DISCUSSION AND CONCLUSION

In robotic microscopy, the large data sets present enormous potential and problems. Here, we present a new approach to analyze and visualize results from these large image sets. The large data sets generated by robotic microscopy require automated image analysis software. ImageA counts the number of cells on an image, determines the levels of fluorescence, and allows visualization of the output on flow cytometry files. Here, we demonstrated the utility of this software by using STS to induce apoptosis and measured levels of annexin-positive cells over time. Direct counting by the software and analysis of the generated flow cytometry output files revealed that this approach was comparable to data generated by flow cytometry. Some notable advantages and disadvantages exist. Flow cytometry advantages include the ability to scan an extremely large population (greater than $1x10^5$ cells) and detect rare events at high speeds and quantify multiple fluorescent signals using an array of lasers at specific wavelengths. Our current method only demonstrated the use of one fluorescent channel; however the only limit on the number of fluorescent signals that can be employed depends on the ability of different signals to be distinguished from each other. Further, because measurement of signal intensities on images was collected using a fluorescent light source over multiple wavelengths, measurement of signal intensity is only pseudo-quantitative. This means that binary decisions such as distinguishing fluorescent objects from non-fluorescent objects or bright fluorescent objects from dim fluorescent objects could be completed. Our software could not be used to determine differences in signal intensities unless properly validated. Flow cytometry can collect data at only one time point from adherent cell populations. Sample size using the live cell microscopy depends on the number of images collected in each group. In these experiments, both methods had sample sizes at each time point on the same order of magnitude. Further, live-cell microscopy has the added benefit of following the population over an extended period of time. This permits the long term observation of trends using a smaller number of cells. This is especially useful in fields where only small populations of cells can be collected, including stem cell biology or working with clonal populations of cells.

Many different technologies and languages exist to conduct image processing or design image analysis software. The largest choice is between writing custom built software or using image analysis software such as the commercial packages Metamorph, ImageMagik, and

Northern Eclipse or open source projects such as ImageJ. Custom built code has the most flexibility, functionality, and ability to be modified. It has the least amount of limitations, but has the disadvantage of requiring the most technical expertise. We developed custom code for this project because the challenges presented by developing this technology required maximum flexibility and functionality. Many different image analysis code libraries or packages exist to construct code, including writing scripts in the available software or Matlab or writing compilable code using the libraries ITK. ITK was chosen because of the advantages of a higher computer language including portability, efficiency, and scalability. Because it is composed of a large library, multiple options exist to perform a single task. Most importantly, it's an open source library that can be compiled on multiple operating systems with an excellent support community.

Both methods of analysis of the fraction of annexin-positive cells collected using live cell microscopy have comparable results to measurements collected using flow cytometry. Some important distinctions and similarities exist. In flow cytometry, annexin-positive cells are classified based on an object having a fluorescent signal above a specified threshold intensity as determined from unstained controls. A similar approach in image analysis is referred to as a binary threshold where objects below a given level are classified as background pixels. The FITC fluorescent channel is thresholded at a given value based on unstained control cells under the same fashion as single parameter controls in flow cytometry. A correct threshold value is easy to determine, as low threshold values generate a large volume of noise and above this initial value, the measurements are not sensitive. From this perspective, the gate has a binary-like behavior. In fluorescence microscopy, noise and cells are distinguished based on the size of the objects similar to the forward and side scatter gating used in flow cytometry (Fig. 10A).

Visual interpretation of time series is typically conducted by displaying the results as a movie. This method has a number of disadvantages including the loss of quantitative information on the image, and the inability to view an image set consisting of thousands of images. Data collected using flow cytometry has a similar problem as high through-put live-cell microscopy. Past groups that have worked with high-throughput microscopy have adopted a method used in microarrays where data is displayed as a heat map (Bahnson et al., 2005; Perlman et al., 2004). In a flow cytometry sample, thousands of events are collected, and measured using an array of parameters that describe fluorescent intensities and cell light scattering properties. A unified,

standard data file format for flow cytometry, flow cytometry standard (FCS), is used that allows data collected on any instrument to be read and analyzed on other computers and software (Seamer et al., 1997). This allows a very large data set to be visualized and analyzed from a global perspective. Our approach to the analysis of images collected on the microscope is similar to the flow cytometry measurement parameters. Following this methods similarity to flow cytometry, the collected output is written to the FCS file format for visualization on flow cytometry analysis software. Output is also sent to a tab-delineated text file to allow analysis using any statistical analysis software. In this study, we used the freely available open source, R-Project.

An additional concern in these experiments involved possible toxicity issues from either of the fluorescent dyes. However, the low levels of cell death observed using both the live-cell microscopy and flow cytometry suggests toxicity is not a major concern (Fig. 12A). These results were confirmed with flow cytometry measurements. We cannot completely rule out the possibility that these dyes may have made the cells more sensitive to damage and primed the cells for cell death at increasing doses of STS. We did observe that higher doses of the PE cell tracking dye would raise levels of apoptosis in control groups, highlighting the importance of the controls in these experiments.

An interesting note includes the delay between the change in cell morphology and the detection of annexin on the cell surface (Supplementary video #1). At all doses above 50nm STS, cells were observed to condense into spherical blobs within an initial 2 hrs after exposure to STS. Both flow cytometry and live-cell microscopy did not detect significant levels of annexin-positive cells until a few hours after this initial observed morphological change. This highlights the importance and value of collecting the fluorescent signal over a continuous period of time while also observing light microscopy morphology changes.

We have used open source software and robotic microscopy to monitor annexin-positive cell fractions over a continuous period of time. To our knowledge, there is no freely available software or open source code that permits output collected from fluorescent microscopy images to be analyzed as flow cytometry data. Here, we used STS to induce cell death to monitor annexin-positive cell fractions as a proof of concept of the technology we have developed. This software has been designed to measure levels of annexin-positive cells, however it is suitable to measure any single-parameter fluorescent signal in a live cell microscopy environment providing

that it is non-toxic to cells and can maintain a stable fluorescent signal. This includes organic fluorophores and fluorescent semiconductor nanocrystals, quantum dots.

3.4 METHODS

3.4.1 Cell Culture

Primary myoblasts used in these experiments were collected using the modified preplate technique (Rando and Blau, 1994). Cells were expanded and cultured in proliferation media which contained Dulbecco's modified Eagle's medium supplemented with 2 mM L-glutamine,1.0mM sodium pyruvate,10% heat inactivated FBS, 10% horse serum, 1% penicillin/streptomycin, and 0.5% chick embryo extract. During experiments, cells were planted at 2500 cells/cm^2 in either 24 or 48 well collagen coated plates for the live cell microscopy assays or in 6 well plates for the flow cytometry measurements.

3.4.2 Apoptosis

Flow Cytometry: To determine levels of cell death after exposure to staurosporine (STS; Sigma), levels of apoptosis and necrosis were measured using flow cytometry. Myoblasts were cultured for 24 hours under normal culture conditions, and then incubated in STS at 37C. For flow cytometry measurements, cells were harvested at 6, 12, 18, and 24 hours using a dilute trypsin-EDTA solution (0.01%; Gibco Laboratories), and quenched with proliferation media. After centrifugation, the cell pellet and collected media was stained with annexin-V FITC according to manufacturer's directions (BD Bioscience). Flow cytometry measuremenst were collected on a FACSCaliber (Becton Dickenson) with standard calibration and one color control for compensation of fluorochromes and analyzed using FlowJo (Treestar, Inc.).

Live Cell Microscopy: Live cell microscopy was conducted using a robotic, automated imaging system (Automated Cell, Inc.). The cell culture imaging system consists of an environmentally controlled biochamber that maintains a humidified, 37°C atmosphere at 5%CO_2

mounted on an inverted fluorescent microscope (Nikon TE 300) with electronically controlled x-y motorized stage (Ludl Electronics, Ltd.) and a motorized focus. The stage can return to each location on a stage with a repeatability of ±1.5μm (Bahnson et al., 2005). Images were acquired using the 20x objective with a total of 200x magnification on a Nikon TE300 inverted microscope with a Photometrics SenSys high resolution (7 x 9 mm, 1036 x 1318 pixel chip) CCD camera (Roper Scientific). Exposure for all images in the PE fluorescent channel was set at 400ms and at 550ms for the FITC fluorescent channel. The biochamber, microscope, and image acquisition system was controlled using Data Collector™ (Automated Cell, Inc). Image analysis was conducted using custom built software as described below.

Images were acquired on a 30 minute interval for a continuous 24hr period on 24 or 48 well plates. The plate layout included triplicate wells for each group tested, and 9 locations were monitored in each well. Each group had approximately 1,300 images in a 24 hour period. To allow fluorescent segmentation of live cells, myoblasts were loaded with 10μM cell tracker red CMTPX (Molecular Probes), for 1.5hrs, washed in PBS, followed by incubation in culture medium for an additional 1.5hrs, and a final wash in PBS. Levels of cell death were monitored by adding 100μg/mL of Annexin-V FITC (BD Clontech) to each well. After an initial set of images at each location in the well were acquired, apoptosis was induced using increasing doses of staurosporine.

3.4.3 Software

The custom designed software used to analyze the images collected from the automated microscopy contains three separate pieces: the GUI, image analysis, and output formatting. Each component of the image analysis software used in this project are open-source. The GUI was written using the QT (version 3.2; Trolltech) a C++ library available under the GNU GPL license available for download (http://www.trolltech.com/download). The image analysis was conducted using the Insight Toolkit (ITK) an open source C++ software library for image segmentation and registration available for download (http://www.itk.org)(Yoo et al., 2002). Both of these toolkits can be compiled on Windows, Apple, and Linux. Output from each image were sent to a tab-delineated text file for statistical data analysis, and later converted to an FCS file format (Seamer et al., 1997) for analysis on the flow cytometry software FLowJo. Similar to flow cytometry,

each object on an image was considered an event. The measurements associated with each event, which roughly corresponds to a cell, were outputted to the flow cytometry standard data storage (FCS) version 3.0 file format (Seamer et al., 1997). This permitted the image processing measurements to be compared to flow cytometry measurements.

The executable files, example images, and the source code are available for download at www.imageK.org, and permanently archived with a digital handle using the Insight Journal, an online, open-peer reviewed journal (http://www.InsightJournal.org/).

3.4.4 Data Analysis and Statistics

All statistical analysis was performed using the open source statistical and data analysis programming environment, R-Project (Team, 2006). Flow cytometry and microscopy data formatted into the FCS file format were analyzed using FlowJo (TreeStar, Inc.).

4.0 ANTIOXIDANT CAPACITY IN MDSC BASED CELL THERAPIES

4.1 INTRODUCTION

Myogenic cells have been proposed as cell sources for both skeletal and cardiac muscle cell based therapies. Diseased myocardial tissue has a limited ability to regenerate, leading to eventual heart failure. As an alternative to heart transplantation, numerous groups have proposed using different cell types as an exogenous source of cells for transplantation into failing heart tissue to improve performance. Similar approaches have been pursued as treatments in muscular dystrophies. Myogenic cells are the fundamental building blocks of a mature skeletal muscle fiber, and are a natural choice in developing a cell therapy treatment.

A major obstacle in both of these therapies is the loss of the majority of transplanted myoblasts shortly after transplantation. This has been documented in cardiac cell transplantation, but closely studied following skeletal myoblast therapies. In skeletal muscle myoblast transplantation, an inflammatory response was observed shortly after injection (Beauchamp et al., 1994; Beauchamp et al., 1999; Fan et al., 1996; Gussoni et al., 1997; Gussoni et al., 1992; Karpati et al., 1993; Mendell et al., 1995). Various groups have postulated that the small number of injected myoblasts that survive the transplantation in both cardiac and myoblast transplantation may be a special subpopulation of cells (Beauchamp et al., 1999; Oshima et al., 2005; Qu et al., 1998; Urish et al., 2005).

The preplate technique was originally developed to isolate myoblasts from the fibroblasts, endothelial, and adipogenic tissue of whole tissue preparations based on the non-myogenic tissue cell types greater adherence to the bottom of a cell culture flask (Jankowski et al., 2002a; Lee et al., 2000; Qu-Petersen et al., 2002). Our group modified this technique to isolate various populations of myogenic cells, including quiescent and activated satellite cells and MDSCs, based on adherence to collagen coated flasks. This final population, MDSCs,

appears to be an early progenitor population of myogenic cells based on the cells' scarcity in muscle tissue and absence of the myogenic markers, including MyoD. There were three unique features with this cell population. First, MDSCs can differentiate into multiple lineages including muscle, bone, epithelial, neural, and hematopoietic lineages (Urish et al., 2005). Second, the cells show multiple signs of long term self-renewal (2005; Deasy et al., 2005; Qu-Petersen et al., 2002). More importantly, when transplanted into skeletal muscle, MDSCs have a superior ability to regenerate skeletal muscle compared to myoblasts (Lee et al., 2000; Qu et al., 1998; Qu and Huard, 2000). Similar results were observed in cardiac cell therapies; MDSCs had superior engraftment and functional improvement compared to transplanted myoblasts (Oshima et al., 2005).

A major unanswered question has been identifying the attributes that give MDSCs a superior ability to repair tissue compared to myoblasts. Stem cells are defined by their ability to differentiate into multiple tissue types and their ability to self-renewal. MDSCs distinct phenotype of relatively high levels of proliferation, a propensity for continued self-renewal, and the ability to act as a single unit capable of regenerating all the different cell types necessary for functional muscle, is a unique property that has been reported to be important in muscle regeneration. However, the dominant role of cell survival in both of these cell transplantations suggests that other factors are important.

The rapid, large-scale initial cell death and presence of inflammation at the site of transplantation in both skeletal muscle therapies suggests that oxidative stress may play an important role in the transplantation process(Urish et al., 2005). Oxygen is part of the crucial step in cellular respiration because of its strong ability to strip and accept electrons from other molecules, however this property is also inherently dangerous to the cell. The destructive power of oxygen is a major component of inflammation. Ischemia and the associated reperfusion injury is directly linked to the production of various reactive oxygen species (ROS) (Ambrosio and Tritto, 1999; Carden and Granger, 2000; Zhao, 2004). After cell transplantation, the mechanical perturbation of the microvascular barrier results in the recruitment of inflammatory cells (mainly neutrophils and monocytes) and in further ischemia (Carden and Granger, 2000; Gute et al., 1998). The induction of oxidative stress leads to the generation of proinflammatory cytokines, including TNF-α, and the ischemia both directly result in oxidative stress (Dhalla et al., 1999; Gute et al., 1998). From this perspective, one of the main outcomes of oxidative stress is the

ensuing inflammatory stress and its associated cytokine storm of TNFα, IL-1, and IL-6. Oxidation is the primary factor responsible for the destruction of protein, lipids, and DNA. It has been shown that inflammation and the associated release of pro-inflammatory cytokines leads to oxidative stress at the local microenvironment after multiple types of cell transplantation, including myoblast transplantation into skeletal and cardiac muscle, transplantation of pancreatic islets, and bone marrow transplantation (Bertera et al., 2003; Blackwell et al., 2000; Bloch and Vardi, 2005; Bottino et al., 2002; Bottino et al., 2004; Evens et al., 2004; Guerette et al., 1997a; Guerette et al., 1997b; Qu et al., 1998; Suzuki et al., 2004; Suzuki et al., 2000).

Here, we compared the ability of MDSCs and myoblasts to resist inflammatory an oxidative stress and the role this played in the regenerative capacity of the cells *in vivo*. We hypothesized that the inflammatory response observed at the site of transplantation is a factor in the large differences observed in the engraftment capacity of MDSCs and myoblasts. Our primary objective was to determine if a phenotypic resistance to stress could be observed between the two cell populations including survival, differentiation, and antioxidant capacity. We also documented differences in cellular damage following exposure to oxidative stress. We then investigated if any of these differences could alter the regenerative capacity of the cells *in vivo*.

4.2 RESULTS

4.2.1 MDSCs Have Lower Levels of Oxidative and Inflammatory Stress Induced Cell Death and Apoptosis

MDSCs have demonstrated an increased regenerative capacity in both skeletal and myocardial muscle (Oshima et al., 2005; Qu-Petersen et al., 2002; Urish et al., 2005). Further, multiple groups have demonstrated a large inflammatory response at the site of both these types of transplantation (Bertera et al., 2003; Blackwell et al., 2000; Bloch and Vardi, 2005; Bottino et al., 2002; Bottino et al., 2004; Evens et al., 2004; Guerette et al., 1997a; Guerette et al., 1997b; Qu et al., 1998; Suzuki et al., 2004; Suzuki et al., 2000). Oxidative stress is a potent stimulant

and amplifies the inflammatory response via nuclear factor kappa B (NFκB) signaling. We hypothesized that MDSCs may have an increased regenerative capacity because of an increased resistance to oxidative stress and the following inflammatory response. To test this hypothesis, myoblasts and MDSCs were exposed to increasing doses of H_2O_2 and TNFα to determine if MDSCs had a survival advantage after exposure to stress.

Each cell population was exposed to increasing doses of H_2O_2 (Fig 14). At each dose, MDSCs had lower levels of apoptosis than myoblasts. MDSCs had slightly higher levels of necrosis, but this was a minor fraction of the total cell death. These results suggested that apoptosis is the dominant form of cell death, and that MDSCs have an increased resistance to oxidative stress induced apoptosis. A limiting factor in these experiments was the ability to only collect a limited series of measurements at one time point.

Our group has adapted a robotic, live-cell microscopy system to measure levels of annexin-positive cells over an extended and continuous time period. Using this approach, it was possible to screen a larger number of doses of H_2O_2 over a continuous time period instead of a limited number of doses at a single time point. MDSCs consistently had lower levels of cell death as compared to myoblasts as both populations were exposed to a range of H_2O_2 (Fig. 14D-H). A summary of these results at 18hrs is included to allow a comparison to results collected using flow cytometry (Fig. 14C). Except at the highest dose of H_2O_2, these results were comparable. However, Figure 14H suggests that the H_2O_2 concentration was approaching a level where MDSCs ability to dissipate H_2O_2 was finally overwhelmed to a similar degree as myoblasts.

Similar results were observed when both cell populations were exposed to increasing doses of the inflammatory cytokine TNF-α. Physiologic concentrations of TNF-α operate in the range of 1 to 5ng/mL. After approximately 18 hrs, myoblasts had significantly higher levels of cell death at all doses (Fig. 15). Together, these results suggested that MDSCs possessed a resistance to stress induced apoptosis. These results were significant, but were not as dramatic as the differences seen between the two cell populations regeneration capacity. This led us to investigate if oxidative and inflammatory stress would alter the levels of differentiation in the two cell groups.

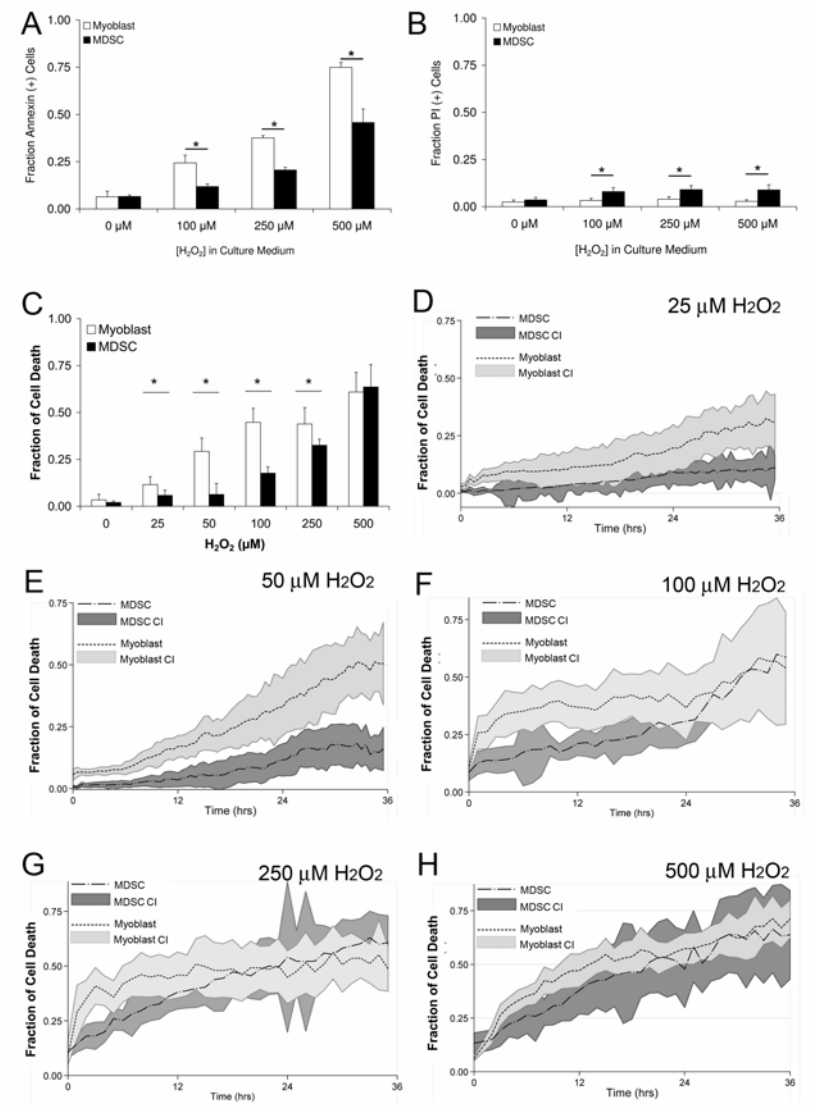

Figure 14: MDSCs have lower levels of cell death following exposure to H_2O_2.
Myoblasts and MDSCs were cultured for 18hrs in increasing doses of H_2O_2, and the levels of apoptosis (A) and necrosis (B) were measured using flow cytometry with Annexin-V and propidium iodide staining. MDSCs had lower levels of apoptosis at all doses (P<0.05). Myoblasts and MDSCs had significantly higher levels of apoptosis than untreated controls (P<0.05). Myoblasts had significantly lower levels of necrosis than MDSCs (P<0.05), however MDSCs levels of necrosis were not significantly higher than untreated controls (P=0.07). Further, comparing the two different types of cell death, apoptosis was the dominant form. An automated live-cell microscopy method was used to monitor levels of Annexin-V staining over a 36hr period in myoblasts and MDSCs at 10 (C), 25(D), 50(E), 100(F), 250(G), or 500µM H_2O_2 (I). Data points were collected every 30 min, and include 27 different measurements in each group. In the plots of C-I, the solid lines represent the mean fraction of annexin-positive cells. The range-plot represents the 95% confidence interval (CI) of these measurements. Statistical analysis was performed using ANOVA.

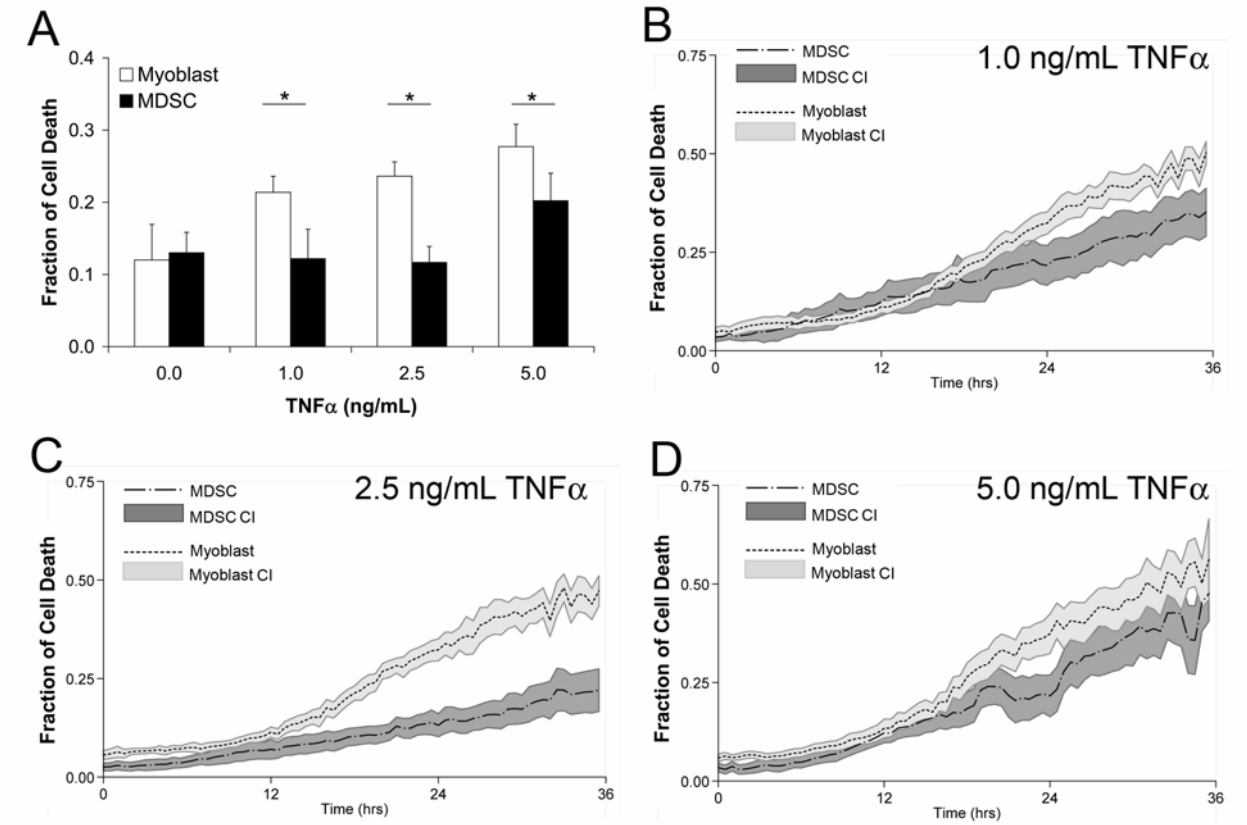

Figure 15: MDSCs have lower levels of cell death following exposure to the inflammatory cytokine TNF-α.

An automated live-cell microscopy method was used to monitor levels of annexin-V staining over a 36hr period in myoblasts and MDSCs at 1.0(B), 2.5(C), and 5.0 ng/mL TNF-α (D). A summary of these results at 18 hours are included (A). Data points were collected every 30 min, and include 27 different measurements in each group. The solid lines represent the mean fraction of annexin-positive cells. The range-plot represents the confidence interval of these measurements. Data points in each cell group were collected every 30 min, and each data point contains 27 independent measurements. As a result, the mean annexin-positive cell fraction is plotted as a line, but the 95% confidence interval (CI) of this line is plotted as a range. This is possible because of the large number of measurements at each of the numerous data points. ANOVA was performed at 18 hrs to determine significant differences ($P<0.05$).

4.2.2 MDSCs Maintain the Ability to Differentiate After Oxidative Stress.

Cell survival is one phenotype that may confer an advantage in muscle repair; however the ability of a cell population to successfully differentiate is also important. As a result, the ability of MDSCs and myoblasts to differentiate, fuse, and form myotubes after exposure to oxidative and inflammatory stress was investigated. After culture in low serum media to induce differentiation, cells were temporarily exposed to increasing doses of H_2O_2 and TNF-α. Differentiation was measured as a function of the fusion index, the ratio of nuclei colocalized with myosin heavy chain, a late differentiation myogenic protein. At day 3, large differences between the ability of MDSCs and myoblasts to form myotubes after exposure to oxidative and inflammatory stress were observed. At increasing doses of H_2O_2, the fusion index of MDSCs remained constant, however myoblasts had a progressive dose response decrease in their fusion index. These responses were temporary, and at day 4 both groups had similar levels of fusion (Fig 16). An identical response was measured when both cell populations were exposed to TNFα (Fig 17). These results demonstrated that MDSC differentiation was not inhibited by these oxidative or inflammatory stresses, but that myoblast differentiation was only temporarily sensitive to this stress.

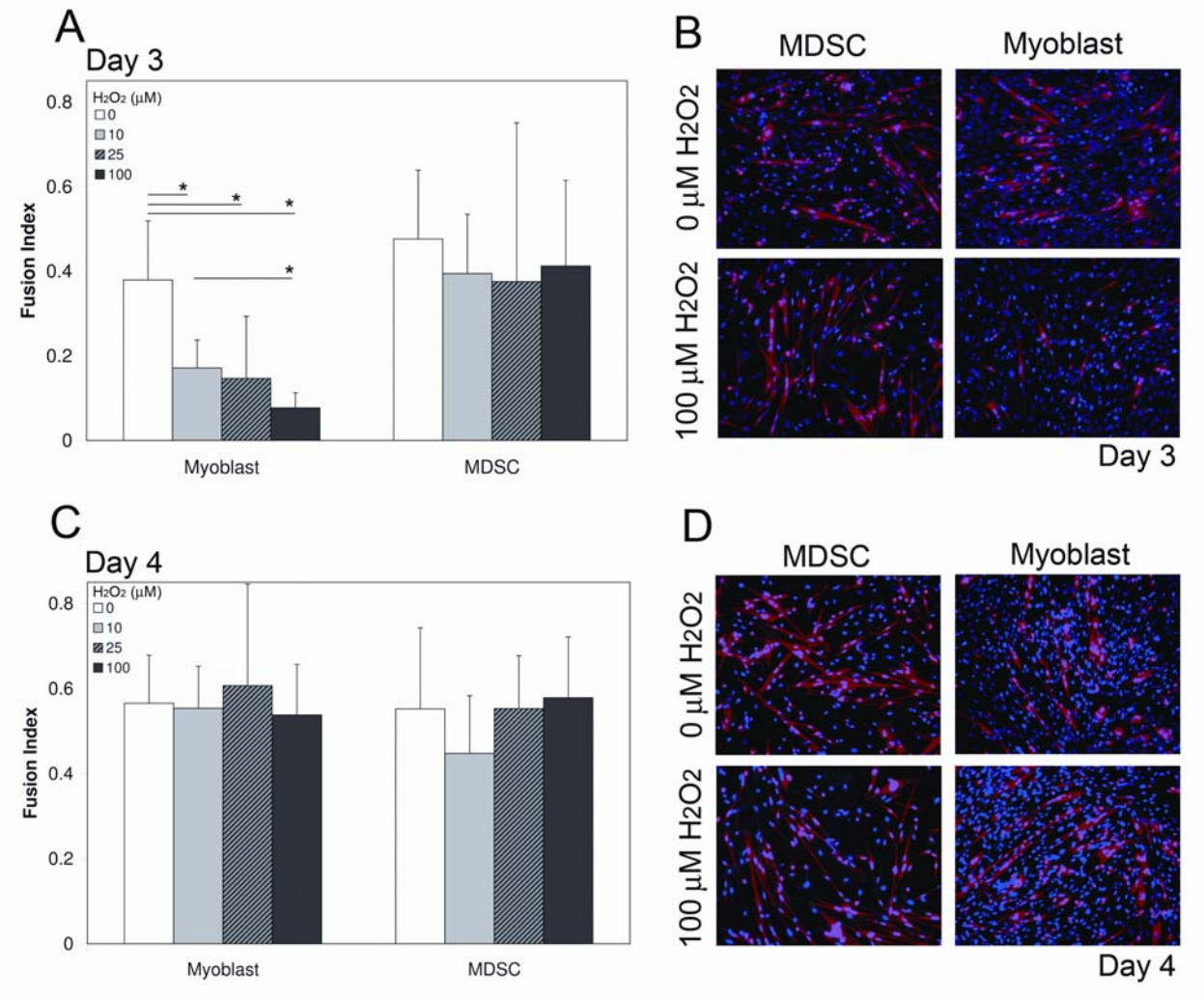

Figure 16: Oxidative stress delays differentiation in myoblasts but not in MDSCs.
Immediately after cultures were exposed to low serum fusion conditions, increasing doses of H_2O_2 were added to the media to induce oxidative stress. After a two day period, this media was replaced with fresh low serum media. Differentiation was monitored by measuring the fusion index – the ratio of nuclei associated with the late fusion myogenic protein, myosin heavy chain (MHC). (A) At day 3, MDSCs exposed to different doses of H_2O_2 had similar levels of fusion as untreated controls. However, myoblasts treated at all doses of H_2O_2 had significantly lower levels of fusion than untreated controls (*P<0.05). Myoblasts treated at the highest dose of H_2O_2 had significantly lower levels of fusion than myoblasts treated at the lowest dose, revealing a dose-dependent response (*P<0.05). (B) Representative images of MDSCs and myoblasts exposed to 0 and 100μM of H_2O_2 at day 3. (C) At day 4, myoblasts and MDSCs exposed to H_2O_2 were not significantly different than untreated controls. (D) Representative images of MDSCs and myoblasts exposed to 0 and 100μM of H_2O_2 at day 4.

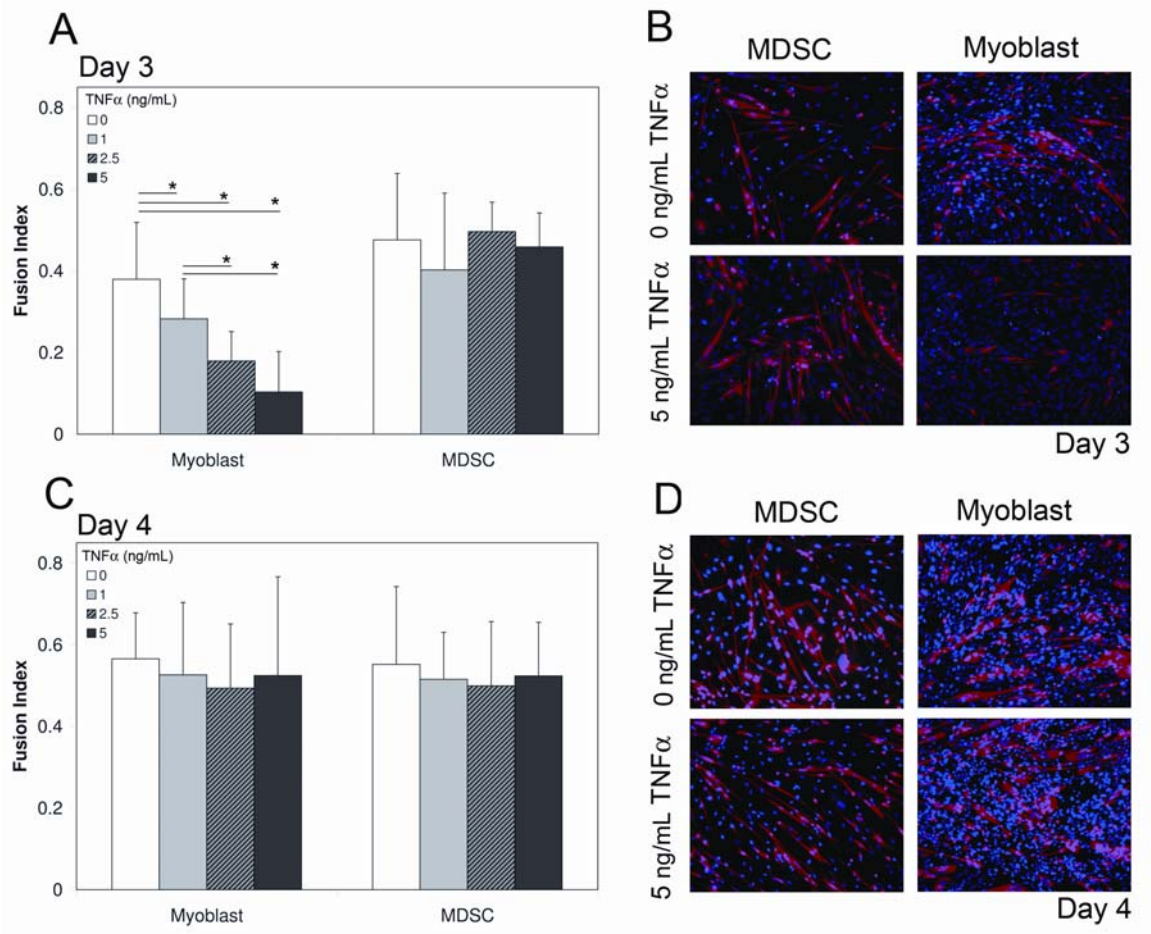

Figure 17: TNF-α delays differentiation in myoblasts, but not in MDSCs.
The fusion index of myoblasts and MDSCs treated with increasing doses of TNF-α were measured. (A) At day 3, myoblasts treated with all doses of TNF-α had significantly lower levels of fusion than untreated controls (*P<0.05). Myoblasts treated at the lowest dose of TNF-α, 1.0ng/mL, had significantly higher levels of fusion than the other two lower doses revealing a dose-dependent response (*P<0.05). At day 3, TNF-α did not alter the levels of fusion of MDSCs. (B) Representative images of MHC expression between MDSCs and myoblasts at day 3. (C) At day 4, TNF-α did not alter the fusion index of myoblasts and MDSCs. (D) Representative images of MHC expression are shown between myoblasts and MDSCs.

4.2.3 Myoblasts Have Higher Oxidative Damage from Increased Intracellular ROS.

MDSCs had lower levels of cell death and maintained their ability to differentiate as compared to myoblasts after exposure to oxidative and inflammatory stress. We hypothesized that these phenotypic differences extended from higher levels of oxidative damage in myoblasts following exposure to oxidative stress. Damage from increased levels of intracellular reactive oxygen species (ROS) can be assessed by measuring oxidative protein, lipid, or DNA damage. Therefore, we first measured levels of intracellular ROS in both cell populations following exposure to a high dose of H_2O_2 using the fluorescent indicator carboxy-H_2DCFDA (Fig. 18A and 18B). At the maximum levels of ROS, MDSCs had essentially no measurable level as compared to the high level of ROS measured in myoblasts. Oxidative damage to proteins was monitored following exposure to multiple doses H_2O_2. Densitometry analysis revealed that MDSCs had lower levels of oxidative protein damage than myoblasts at respective doses (Fig. 18C). Although, these differences were not statistically significant, the same trend was measured in three separate experiments.

4.2.4 MDSCs Have Increased Protection from Reactive Oxygen Species

Increased levels of ROS and oxidative damage imply that MDSCs have higher levels of antioxidant activity to defend against redox imbalances. The two major cellular antioxidants are glutathione (GSH) and the multiple types of superoxide dismutase (SOD). Basal concentrations of reduced glutathione (GSH) were measured using flow cytometry analysis following staining with monochlorobimane (MCB). The histogram plot of both cell groups reveal that the MDSCs have a shifted peak compared to myoblasts, but also shows that MDSCs have a skewed distribution towards that higher intensity of fluorescence (Fig. 18D). Mean fluorescence reveals that the differences in GSH levels are significant (Fig. 18E). Total SOD activity was measured between both cell groups using a colorimetric assay. Similar to GSH levels, MDSCs had higher levels of total basal SOD activity (Fig. 18F).

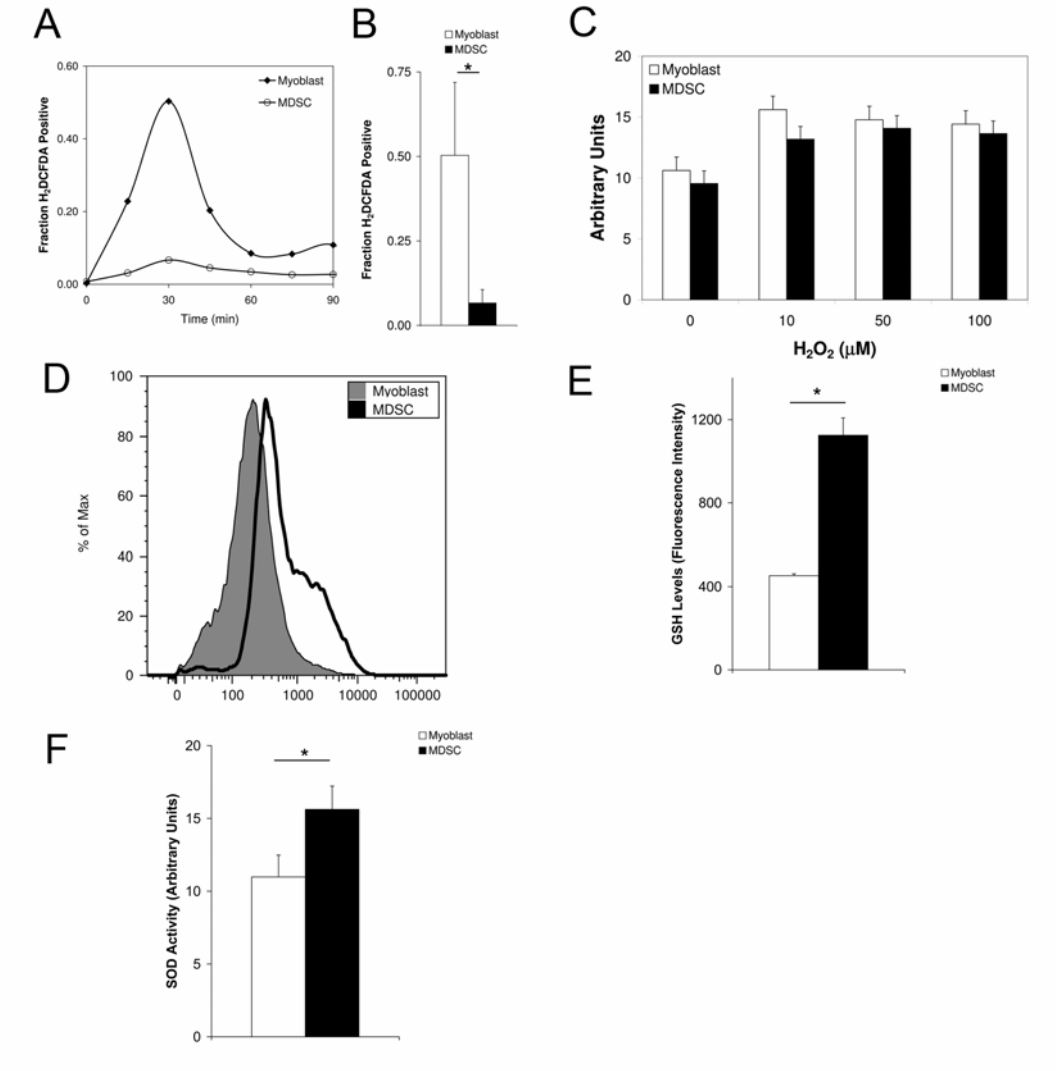

Figure 18: MDSCs have lower levels of oxidative damage and a higher antioxidant capacity than myoblasts.

Both cell populations were exposed to 100μM H_2O_2 for 24hrs. (A) Intracellular levels of ROS were measured in the initial 2hr period following exposure to 500μM H_2O_2. MDSCs had little increase in ROS while myoblasts had a large increase in intracellular ROS at 30 min. (B) The differences observed at 30 min were significant (*P<0.05). (C) Both cell populations were exposed to multiple doses of H_2O_2 up to 100μM for 24hrs, and levels of protein oxidative damage were measured. Protein oxidative damage was measured using DNPH-derivitization, probing with appropriate antibodies, and conducting electrophoresis. Densitometry of the results shoed myoblasts had higher levels of oxidized protein damage, but these difference were not significant. (D) Both populations were stained with MCB to determine levels of GSH, an important cellular antioxidant. The flow cytometry histogram revealed that MDSCs had a shifted and skewed population density to higher levels of GSH. (E) The mean of the fluorescent intensity of the histogram peaks are shown (*P<0.05). (F) MDSCs had a significantly higher total activity level of SOD (P<0.05).

4.2.5 Decreasing the MDSCs Resistance to Stress Dramatically Decreases the Regeneration Capacity of MDSCs

Compared to myoblasts, MDSCs increased antioxidant capacity prevents oxidative and inflammatory stress induced apoptosis or a decrease in differentiation. To assess the role this antioxidant capacity plays *in vivo*, we performed a series of experiments to inhibit the MDSCs resistance to oxidative stress and measure any possible change on the level of regeneration. Diethyl maleate (DEM) is a specific, non-protein thiol-depleting agent that selectively inhibits glutathione activity (Plummer et al., 1981) In initial experiments, the basal levels of GSH were measured following exposure to increasing doses of DEM. Levels of either 50 or 100 μM of DEM were found to sufficiently lower levels of MDSC GSH to levels comparable to those of myoblasts (Fig. 19A). Further, MDSCs were exposed to multiple doses of DEM, and levels of apoptosis and changes in differentiation were compared to untreated MDSCs and myoblasts. At 100μM of H_2O_2, MDSCs exposed to 50μM DEM had similar levels of cell death and changes in fusion as compared to the myoblast population (Fig. 19B). Thus, 50μM of DEM was selected as an appropriate dose to inhibit the MDSCs resistance to oxidative stress and make the MDSCs comparable to myoblasts.

To determine the role oxidative stress plays in dystrophin-positive myofiber regeneration, equal numbers of untreated MDSCs and MDSCs treated with 50μM of DEM were injected into the gastrocnemius of dystrophin deficient mdx mice (MDSCs treated with DEM, n=8; untreated MDSCs, n=8; untreated myoblasts, n=8). After two weeks, the regeneration index (number of dystrophin-positive myofibers normalized to $1x10^5$ injected cells) was measured. On observation, MDSCs contained much larger dystrophin-positive myofiber engraftments than MDSCs treated with DEM (Fig. 19C). When the engraftments were analyzed, MDSCs treated with DEM produced dystrophin-positive engraftments significantly smaller than untreated MDSCs and comparable to myoblasts (Fig. 19D; MDSC vs myoblast, $P<0.05$; MDSC+DEM vs myoblast, $P=0.072$; MDSC vs MDSC+DEM, $P<0.05$). When antioxidant levels are similar between the two cell populations, the ability to regenerate dystrophin-positive myofibers is comparable.

These results suggest that a cell's antioxidant capacity and the ability to dissipate oxidative stress is a major phenotype important in the regenerative capacity of a cell. This

hypothesis was tested in a second type of regenerative therapy. Myoblasts have been used in multiple clinical trials as a cell therapy to preserve cardiac function following myocardial infarctions. To assess if MDSCs antioxidant capacity played a role in cardiac cell therapies, the right main coronary artery was permanently ligated to induce a myocardial infarction in adult wild-type C57 mice, and cells were transplanted immediately after ligation (MDSCs+DEM, n=8; MDSCs, n=7; PBS control, n=8). Histological analysis was completed at 8 weeks, and confirmed the myocardial infraction and resulting fibrosis (Fig 20A-C). To compare left ventricle (LV) function and remodeling, echocardiography was performed at 6 weeks after infarction. No differences in LV cavity size were observed between all three groups as assessed by end-diastolic area (EDA; data not shown). Systolic function was also assessed by measuring the fractional area change (FAC) (Fig. 20D). Both cell treatment groups showed significantly better systolic function relative to that of the PBS control group (MDSC vs myoblast, $P<0.05$; MDSC+DEM vs PBS, $P<0.05$). However, MDSC showed significantly better systolic function than MDSC treated with DEM (MDSC vs MDSC+DEM, $P<0.05$).

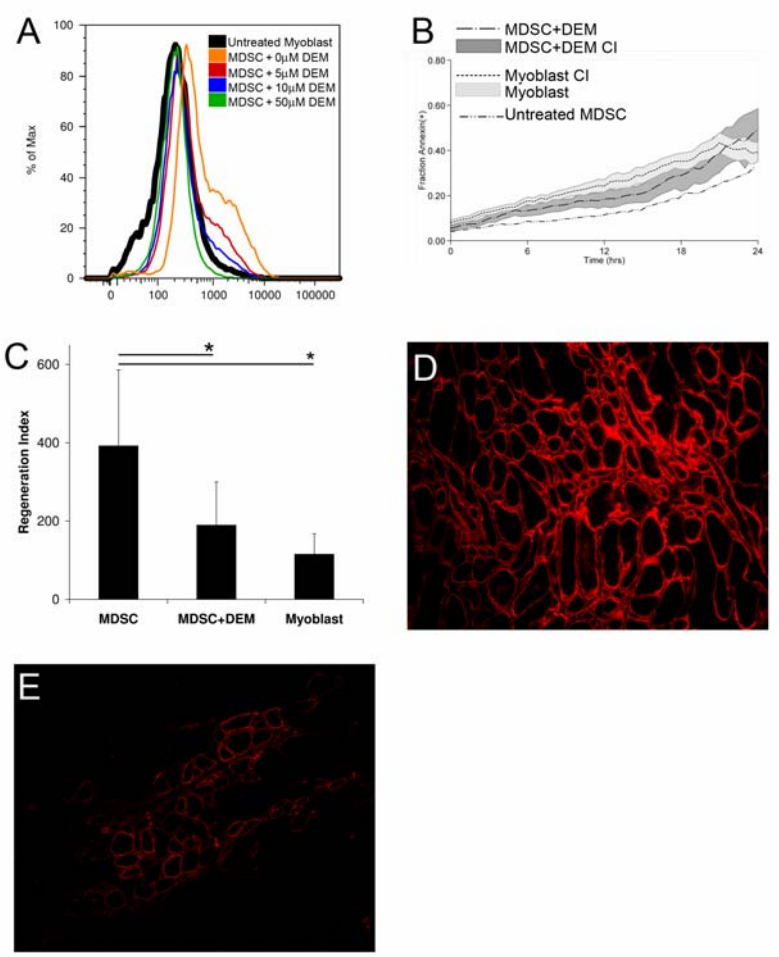

Figure 19: Decreasing the levels of GSH in MDSCs decreases the ability of MDSCs to regenerate dystrophin-(+) myofibers.

Decreasing the levels of GSH in MDSCs decreases the ability of MDSCs to regenerate dystrophin-(+) myofibers. A series of experiments were conducted to identify the appropriate dose of DEM that would decrease the antioxidant capacity of MDSCs to comparable levels of myoblasts. (A) The histogram plots of GSH levels of MDSCs treated with increasing doses of DEM and untreated myoblasts. (B) The levels of cell death of MDSCs treated with 50 μM DEM and untreated myoblasts after exposure to 100μM H_2O_2. The area associated with each line represents the 95% confidence interval (CI) of the respective mean. As a reference, levels of cell death of untreated MDSCs exposed to 100μM H_2O_2 are shown. The CI of this line is not included to increase clarity. After these two experiments, a dose of 50μM of DEM was selected to decrease the antioxidant capacity of MDSCs to levels comparable to myoblasts. MDSCs treated and untreated with 50μM of DEM were injected into the skeletal muscle of the mdx mice (n=8), sacrificed at 2 weeks, and the regeneration index measured. (C)Treated MDSCs had significantly lower regeneration indexes as compared to untreated MDSCs and similar levels of regeneration index as compared to myoblasts (*P<0.05). Representative images of the dystrophin-positive engraftments of MDSCs (D) and myoblasts (E) are shown.

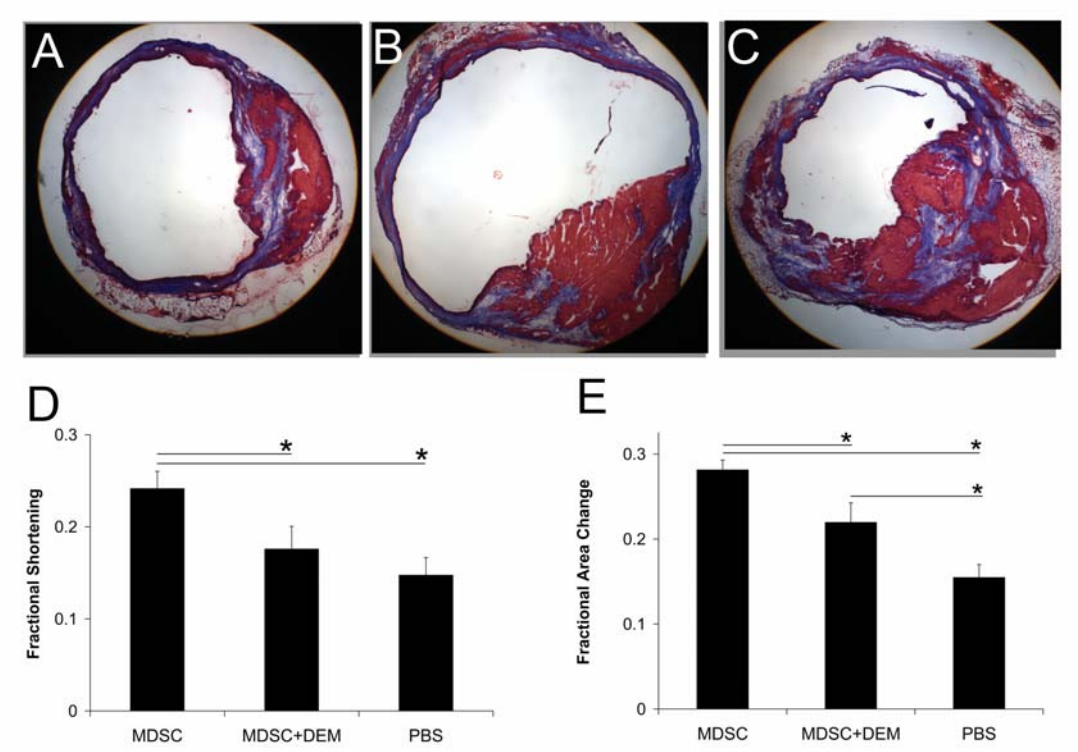

Figure 20: Decreasing the levels of GSH in MDSCs decreases the ability of MDSCs to improve cardiac function following induced myocardial infarction.
Cardiac section from induced myocardial infarctions reveal areas of fibrosis in (A) PBS control (B) MDSCs treated with 50μM DEM (C) MDSCs. Echocardiography was used to measure the fractional shortening (D) and fractional area change (E) of the three groups. MDSCs had significantly higher changes in FS and FAC than MDSCs treated with DEM or the PBS control. MDSCs treated with DEM only had significantly higher FAC than the PBS control ($P<0.05$)..

4.3 DISCUSSION AND CONCLUSION

Multiple cell populations have been investigated in clinical and preclinical trials for dystrophic and cardiac muscle cell therapies. In this study, we have investigated the possible role of a stem cell's antioxidant capacity in its regenerative capacity. Previous reports have shown that MDSCs, an early myogenic progenitor cell population, have a superior ability to regenerate dystrophin-positive myofibers in dystrophic skeletal muscle as compared to myoblasts. Additional studies have shown that similar patterns exist in the myocardial infarct model; transplanted MDSCs have an improved ability to increase functional recovery of myocardial muscle following an induced ischemic episode as compared to myoblasts. Here, we have demonstrated a possible explanation outlining these differences in the regenerative capacity of the two myogenic cell populations. MDSCs have shown decreased levels of oxidative stress induced apoptosis while myoblasts have shown a decreased ability to differentiate following these same conditions. These differences can be explained by a protection against oxidative damage. Myoblasts showed higher levels of reactive oxygen species, oxidative protein damage, and oxidative lipid damage following exposure to oxidative stress. These levels of damage appear to be higher in myoblasts as compared to MDSCs because myoblasts have lower levels of GSH and SOD. Finally, when MDSC levels of GSH are reduced to similar levels as myoblasts, MDSC have a dramatic decrease in the ability to regenerate dystrophin-positive myofibers in skeletal muscle and in the functional ability of ischemic myocardial muscle.

Myoblasts and MDSCs can be isolated based on their differential adhesion characteristics, and distinguished based on varying degrees of myogenic commitment and regeneration capacity. Myoblasts isolated by their early adhesion to culture flasks have express high levels of the myogenic markers desmin and pax-7, and a decreased ability to regenerate dystrophin-positive myofibers in dystrophic muscle. In contrast, MDSCs are isolated by their late adhesion to culture flasks, and have low levels of expression of myogenic markers, suggesting that they are less differentiated myogenic precursor (Urish et al., 2005). The most notable difference between these two populations is their dramatic difference to regenerate skeletal and

cardiac muscle. In the dystrophic animal model of Duchenne Muscular Dystrophy, the *mdx* mouse, MDSCs have been shown to have an increased ability to regenerate dystrophin-positive myofibers when injected in skeletal muscle(Deasy et al., 2005; Lee et al., 2000; Qu-Petersen et al., 2002; Urish et al., 2005). Following induced ischemic myocardial infarctions in the murine animal model, a similar pattern was found; MDSCs had an improved ability to restore functional recovery as compared to myoblasts (Oshima et al., 2005).

Several studies have reported that a large percentage of cells die in the short time period after transplantation into both skeletal and myocardial muscle. In skeletal muscle myoblast transplantation, initial work revealed that a large majority of transplanted cells were lost in the initial 24hrs (Beauchamp et al., 1994; Fan et al., 1996; Huard et al., 1994a), and long term analysis showed that less than 5% of the total number of injected cells survive transplantation after one month (Beauchamp et al., 1999; Gussoni et al., 1997; Gussoni et al., 1999; Karpati et al., 1993). In the heart, multiple types of transplanted cells have a large percentage of cells that die shortly after transplantation including myoblasts (Menasche, 2004; Suzuki et al., 2000; Taylor et al., 1998), cardiomyocytes (Zhang et al., 2001), hematopoietic stem cells (Balsam et al., 2004, Murry et al., 2004), and mesenchymal stem cells (Mangi et al., 2004). MDSCs have been described as a unique cell population because of their ability to avoid this initial pitfall following transplantation in skeletal muscle (Qu and Huard 2000; Qu et al., 1998; Qu-Petersen et al., 2002) and myocardial muscle (Oshima et al., 2005).

A large initial loss of transplanted cells strongly suggests a primary non-function mechanism from damage occurring during either the pre or post transplantation process. In pancreatic islet transplantation, oxidative stress from the transplantation process prior to implantation results in a large decrease in yield of functional islets (Bottino et al., 2004). At the site of skeletal myoblast transplantation, an acute inflammatory response occurs (Urish et al., 2006). Similarly, a rapid and strong inflammatory process is the pathologic hallmark after a myocardial infarction. A major source of the destructive power of inflammation is the direct and indirect generation of reactive oxygen species and free radicals from the release of cytokines and interleukins. Together, this suggests that MDSCs may overcome this initial cell loss from having an increased resistance to oxidative stress.

If multiple groups have demonstrated an inflammatory response at the site of skeletal and myocardial engraftment, we postulated that perhaps one of the mechanisms behind MDSCs

superior regenerative capacity as compared to myoblasts might involve a resistance to this stress. In our initial investigation, we attempted to characterize any differences in the phenotypic ability to resist stress between these two cell populations, namely by measuring levels of survival and differentiation after exposure to stress. Myoblasts consistently had higher levels of cell death following exposure to both H_2O_2 and TNF-α (Fig 16 and 17).These results demonstrated that MDSCs, at a minimum, handled oxidative stress and inflammation differently than myoblasts. However, although promising, these differences were not enough to convince the authors that MDSCs survival advantage over myoblasts entirely explained the observed regenerative differences between the two cell populations. Next, we investigated if oxidative stress and inflammation altered levels of fusion and differentiation.

MDSCs had no change in the ability to fuse and form myotubes after exposure to inflammatory stress. Myoblasts exposed to increased levels of oxidative stress and inflammatory cytokines had a temporary decrease in the ability to differentiate, and when this stress was removed, myoblasts resumed differentiation (Fig 16 and 17). These effects could be extended if myoblasts were continually exposed to TNF-α (Fig 17). This is an important note because different groups have reported that oxidative stress can either induce a "differentiation check point" (Puri et al., 2002) or permanently force a cell into a state of senescence (Stoeber et al., 2004). A "differentiation check point" is similar to a cell cycle check point in that cell division or differentiation is arrested until the damage has been repaired and the stress has been removed. The temporary arrest of cell differentiation that we observed has been previously described. Multiple groups have observed that myogenic differentiation is inhibited after exposure to the inflammatory cytokines TNF-α or IL-1 through activation of the nuclear factor kappa B (NF-κB) pathway (Langen et al., 2004; Langen et al., 2001; Guttridge et al., 2000). Other groups have shown that direct exposure to oxidative stress inhibits myoblast differentiation through the same NF-κB mechanism (Catani et al., 2004). This previous work supports our observations, but also suggests a more direct molecular mechanism of MDSCs' improved regenerative capacity. If myoblast differentiation is inhibited via the NF-κB pathway, this implies that MDSCs maintain normal levels of differentiation after exposure to stress because they avoid NF-κB activation. Indeed, preventing this pathway's activation has been shown to have a remarkable improvement on pancreatic islet transplantation (Bottino et al., 2004). Finally, the continued ability to inhibit myoblast differentiation implies that a sustained inflammatory response will prevent myoblast

differentiation. This is a possible major component of the mechanism for the observed differences in regenerative capacity between MDSCs and myoblasts.

The phenotypic differences in survival and differentiation could be explained by the antioxidant capacity of each population. The two major components protecting a cell from oxidative damage include GSH and SOD. MDSCs had increased levels of both of these components. The increased protection from ROS in the MDSC population resulted in lower levels of intracellular ROS and oxidative protein damage following exposure to oxidative stress (Fig. 18). Other progenitor and stem cell populations have been reported to have increased antioxidant capacity (Dernbach et al., 2004; He et al., 2004). These groups have shown that increased expression of manganese SOD was primarily responsible for an increased resistance to stress. Our study was not designed to identify a single factor responsible for the increased resistance to stress, but did demonstrate that increased expression of multiple antioxidant species. Further, it ahs been demonstrated that depleting levels of GSH in myoblasts has been shown to increase NF-κB activation and inhibit myogenesis supporting a possible link as discussed above (Ardite et al., 2004). It appears that both antioxidant compounds have demonstrated a contribution to improving a cells resistance to inflammation.

The finding that a population of stem cells has increased resistance to oxidative stress has been described to different degrees in the past (Dernbach et al., 2004; He et al., 2004). Other studies have implied the importance of stress in the transplantation process by genetically engineering the transplanted cell population with protection against inflammation and stress, most notably with heat shock proteins. However, no previous work has been completed that directly outlines the role that a phenotype of increased resistance to redox stress plays in regeneration capacity of transplanted cells in vivo to the authors' knowledge.

If MDSC's antioxidant capacity played an important role in their ability to regenerate dystrophin-positive myofibers and improve cardiac function, we reasoned that removing this protection should decrease the cell population's regenerative capacity. MDSCs had higher levels of both antioxidants, however there appeared to be a much greater difference in levels of GSH. DEM is a GSH depleting agent that conjugates with GSH and further removes it by the GSH-S-transferase catalyzed reactions. These effects are only temporary as the cell's machinery to regenerate GSH is still functional. We used DEM to decrease levels of GSH in MDSCs to similar levels as myoblasts. To verify that MDSCs did indeed have a similar resistance to stress,

we confirmed that MDSCs treated with the titrated dose of DEM gave them similar levels of survival and differentiation after exposure to a fixed dose of H_2O_2 (Fig 19). After a dose of DEM was identified that decreased the antioxidant protection of MDSCs to similar levels of myoblasts, we compared changes in the regenerative capacity of the cell population. In dystrophic skeletal muscle, MDSCs treated with DEM had comparable levels of regeneration as myoblasts and decreased levels of regeneration as untreated MDSCs. In ischemic cardiac tissue, MDSCs treated with DEM had less functional improvement than MDSCs. Levels of improvement of the MDSC group treated with DEM were comparable to previous reports of the limited improvement of myocardial function obtained transplanting myoblasts into the ischemic area.

4.4 METHODS

4.4.1 Cell Isolation and Culture

Myoblasts and MDSCs were prepared using a modified version of the preplate technique from three week C57 mice (Qu et al., 1998; Qu and Huard, 2000; Rando and Blau, 1994; Richler and Yaffe, 1970). All cells were cultured and expanded in proliferation media which contained Dulbecco's modified Eagle's medium, 10% fetal bovine serum, 10% horse serum, 1% penicillin/streptomycin, and 0.5% chick embryo extract (Qu-Petersen et al., 2002). Myoblasts were cultured for less than 3 passages prior to each experiment. MDSCs were under passage 20. It is important to note that recent work has described that MDSCs can be cultured past the Hayflick limit for more than 200 doublings without any oncogenic or transformed properties, and still maintain their same regeneration ability as early passages (Hayflick 1960s, DEASY 2005). Antibodies specific for Pax7 (Developmental Studies Hybridoma Bank, Iowa City, IA, USA) and desmin (Sigma, St. Louis, MO, USA) were used as myogenic lineage-specific markers (Qu-Petersen et al., 2002). All Pax7+ or desmin+ cells were counted in both cell populations.

4.4.2 Fusion Index

The rate and degree of fusion was monitored in each cell population after incubation with H_2O_2 and TNFα. Cells were plated at an initial plant density of 1,250 cells/cm^2 in 48 well collagen coated plates, and cultured in high-serum, proliferation media. After 48 hrs, to induce differentiation the culture medium was replaced with low-serum medium containing 2% fetal bovine serum and 1% penicillin/streptomycin in Dulbecco's modified Eagle's medium. Immediately following incubation in the differentiaion medium, cell's were exposed to H_2O_2 (10, 25, 50, and 100μM; Sigma) and TNFα (1.0, 2.5, and 5.0 ng/mL; R&D Systems) to simulate oxidative and inflammatory stress. Media was replaced every two days with fresh differentiation media. After the initial stress, cell's were not exposed to additional H_2O_2 or TNF-α unless otherwise noted.

At day's 0, 2, 3, and 4, plates were fixed in cold methanol, and fields were randomly selected and evaluated for the levels of fast myosin heavy chain-positive myofibers and counterstained with DAPI (Sigma). These images were used to measure the fusion index (Jankowski et al., 2002a) defined as the ratio of the total number of nuclei in myosin-heavy chain compared to the total number of nuclei of the entire cell population. Three wells were used at each time for each dose of either H_2O_2 and TNFα, and 6 fields were randomly selected in each well. This large number of images collected over an extended time period were analyzed using ImageFi, an open source, freely available program as described below in the image analysis methods section.

4.4.3 Apoptosis

To determine levels of cell death after exposure to oxidative stress, levels of apoptosis and necrosis were measured using flow cytometry. MDSCs and myoblasts were cultured for 24 hours under normal culture conditions, and then incubated in H_2O_2 (100, 250, and 500 μM) at 37C. After 15 hrs, the media was collected, the cells were washed in PBS, harvested in 0.01% trypsin-EDTA (Gibco Laboratories), and quenched with proliferation media. After centrifugation, the cell pellet and collected media was stained with annexin-V and propidium iodide according to manufacturer's directions (BD Bioscience). Levels of apoptosis and necrosis were measured

using flow cytometry (FACSAria; FACSDiva Software; BD Bioscience) with standard calibration and one color control for compensation of fluorochromes. Total cell death was determined as the sum of necrotic and apoptotic cell death fractions normalized to exclude cellular debris.

To monitor the levels of cell death over a continuous time period, a modified live cell microscopy technique was used to measure percentages of annexin-V positive cells. Cells were planted at an initial plant density of 2000 c/cm^2 on collagen Type-I 24 well plates, and cultured for 24 hrs. Cells were loaded with Cell Tracker Red-CMTPX (Molecular Probes) according to manufacturer's directions to aid in segmentation of the entire cell population. Cells were then placed in proliferation media containing 15 μg/mL of Annexin-V FITC (BD Bioscience) and 10 μg/mL of propidium iodide. A microscope imaging system (Automated Cell, Inc) was used to acquire light and fluorescent time-lapsed images on a 30 min time interval (Bahnson et al., 2005; Deasy et al., 2002). At each time point, 9 images in each plate were collected resulting in over 45,000 images being collected in each experiment with each experiment averaging over 1-3x10^5 events being recorded. After an initial baseline measurement was collected, cells were incubated with increasing doses of H_2O_2 (10, 25, 50, 100, 250, and 500 μM; Sigma) and TNFα (1.0, 2.5, and 5.0 ng/mL; R&D Systems). Images were collected on a 30min interval over a 24-36hr time period. The percentages of annexin-positive cells in each population at each time period were measured using open source software. Further details are noted below.

4.4.4 Oxidative Damage

Protein oxidative damage was measured using the oxyblot oxidized protein detection kit (Chemicon) following the manufacturer's protocol with important details and exceptions noted below. Myoblasts and MDSCs were seeded at 2000 c/cm^2, exposed to 0, 10, 50, and 100 μM H_2O_2, after 24hrs, and harvested after an additional 24hrs. Protein concentrations were measured using the bovine serum albumin assay (Pierce). After 60μg of each sample were derivitized with DNPH, one dimensional electrophoresis was conducted on a 4-20% precast SDS/polyacrylamide gel (Bio-Rad). Proteins were transferred to nitrocellulose membranes, incubated in anti-DNPH and appropriate secondary antibody, and developed using a chemiluminescence detection system (Pierce). Following oxyblot analysis, the same membrane was stained for beta-actin as a control

to ensure similar levels of protein were loaded across each lane. Densitometry was performed on each lane using two-dimensional integration with local background substraction, and corrected relative to differences in the beta-actin band intensity.

4.4.5 Antioxidant Capacity

The ability of each cell population to avoid damage from oxidative stress was assessed by measuring the levels of free radicals, reduced glutathione, and levels of super oxide dismutase activity. Levels of reactive oxygen species were measured using 5-(and-6)-carboxy-2′,7′-dichlorodihydrofluorescein diacetate (carboxy-H_2DCFDA; Molecular Probes). Carboxy-H_2DCFDA is a non-polar, nonfluorescent compound that freely crosses the cell membrane, and becomes charged and cell permanent over short time periods after hydrolysis with intracellular esterases. Oxidation following interactions with intracellular reactive oxygen species (ROS) results in conversion to 2',7'-dichlorofluorescein, a highly fluorescent compound. This change in fluorescence can be monitored using flow cytometry using appropriate single parameter controls. Briefly, cells were planted at 2500 c/cm^2, and after 48 hours loaded with 5μM carboxy-H_2DCFDA for 30 min in proliferation media, washed, and exposed to 500 μM H_2O_2. At 15min time intervals, cells were harvested, and green fluorescence was immediately measured using flow cytometry (Hempel et al., 1999).

Levels of reduced glutathione (GSH) were monitored using monochlorobimane (MCB; Molecular Probes), a nonfluorescent bimane that reacts with free GSH to form a highly fluorescent derivative. Cells were loaded with 4μM of MCB for 30 min in proliferation media, harvested, washed, and the fluorescence was measured using flow cytometry with single parameter controls.

Total activity of superoxide dismutase (SOD) was measured using a colorimetric assay (Chemicon, APT290). Myoblast and MDSC cell samples containing 2x10^6 cells were homogenized using a lysis buffer (10mM Tris(pH7.5), 150mN NaCl, 0.1mM EDTA, 0.5% Triton X-100) and centrifuged at 12000 x g for 10 minutes to collect cell lysate. The lysate supernatant was then alloquated into a xanthine/xanthine oxidase solution which produces the superoxide ion. A chromagen molecule binds to superoxide ion and can then absorb light at a 490nm wavelength. Increasing superoxide concentration and therefore chromagen absorbance

indicates decreasing SOD activity. SOD activity was quantified by generating a standardized absorbance curve of increasing concentrations of purified SOD in the same solution.

4.4.6 GSH Depletion

To asses the role of GSH in the MDSC regenerative capacity, MDSCs were depleted of cellular GSH using diethyl maleate (DEM). After 48 hours in standard culture conditions, cells were treated with 50 μM DEM for 2 hrs, washed twice in PBS, and then cultured in fresh proliferation media. In some *in vitro* experiments, multiple doses of DEM were tested. In these cases, cell population levels of GSH were depleted using an identical protocol as desribed above at various doses of DEM as described in the results.

4.4.7 Cell Transplantation

All animal surgical procedures were approved by The Institutional Animal Care and Use Committee, Children's Hospital of Pittsburgh (Protocol 7/03). MDSCs and myoblasts were injected into mdx mice as initially described(Lee et al., 2000; Qu-Petersen et al., 2002). Briefly, $2x10^5$ viable cells were injected into the gastrocnemius muscle of 4-6 week old mdx mice (C57BL/10ScSn DMDmdx/J, The Jackson Laboratory) suspended 30μL of PBS. The mice used in the experiment were not immunosupressed, and the injected muscle was not injured before or after transplantation.

Coronary ligation and cell transplantation into infarcted hearts were performed in 14 week C57BL/10J; The Jackson Laboratory) as previously described (Oshima et al., 2005). Briefly, myocardial infarctions were induced by ligating the left anterior descending coronary artery 2mm from the left auricle. Immediately after ligation, $3x10^5$ cells were injected into the anterior and lateral aspects of the wall bordering the infarct and into the center of the infarct in 30μL of PBS (10μL per region). Mice were anesthetized using 1.0–1.5% isoflurane (Abbott Laboratories, North Chicago, IL, USA) in 100% O2 gas. In the control group, the identical procedure was used, except only PBS and no cells were injected. Echocardiography was performed at 6 weeks, and mice were sacrificed at 8 weeks for histological analysis.

Echocardiography was performed as previously described (Oshima et al., 2005). Briefly, analysis was completed by a blinded investigator using a Sequoia C256 system (Acuson, Mountain View, CA, USA) equipped with a 13-MHz linear-array transducer (15L8). Isoflurane gas was used to anesthetize the mice. It should be noted that although isoflurane gas may have a cardiodepressant effect, other groups have reported that echocardiographic assessment of cardiac function in mice anesthetized with isoflurane is comparable to that in unanesthetized mice (Takuma et al., 2001). Two dimensional images were obtained at the midpapillary muscle level. EDD was measured from at least six consecutive beats using the M-mode tracing. End systolic area (EAS) and end diastolic area (EDA) were determined from short axis images of the left ventricle. The fractional area change (FAC) was calculated as FAC = [(EDA-ESA)÷EDA]

4.4.8 Histological Analysis

Skeletal muscle and hearts were harvested at the indicated time points, and frozen in 2-methylbutane precooled in liquid nitrogen. Skeletal muscle was serially cross sectioned in 10 μm thick sections, and heart was serial cross sectioned from the apex to the base into sections 10 μM thick. Skeletal muscle sections were stained for dystrophin-positive myofibers as previously described(Qu-Petersen et al., 2002). Cardiac sections were stained for the skeletal muscle-specific marker, myosin heavy chain to measure the engraftment area of transplanted cells. The area and size of infarction were identified and measured using the trichrome stain (Sigma). All fluorescence and bright field microscopy was performed using either a Nikon Eclipse E800 microscope equipped with a Retiga EXi digital camres (Q Imaging, Burnaby, BC, Canada) or a Leica DMIRB microscope with a Retiga 1300 digital camera (Q Imaging). All images were adquired with Northern Eclipse software (v6.0; Empix Imaging, Inc., Cheektowaga, NY, USE).

4.4.9 Image Analysis

Image analysis was conducted as noted above to measure levels of apoptosis over a continuous time period (ImageApop) and to measure the fusion index (ImageFI). All programs were written as open source, freely available code using the Insight Toolkit (ITK), an image segmentation and

registration C++ code library (Yoo et al., 2002). The programs and source code used for analysis have been permanently archived on the Insight Journal.

4.4.10 Statistical Analysis

Data is expressed as a mean ± standard deviation, except were noted. Direct comparisons between two cell populations were made using an unpaired, two-tailed Student's *t*-test. Statistical significance was determined if $P<0.05$. All statistical tests were completed using R (R Core Development Team, 2006). Multiple group comparisons were made using two-way ANOVA, using the Student-Newman-Keuls pairwise comparison to determine significance levels.

5.0 CONCLUSION

5.1 SPATIAL TEMPORAL REAL TIME CYTOMETRY

An interesting new technology developed during this project was conducting live-cell microscopy analysis similar to flow cytometry. Future work will include expanding the capacity of this software so that cell populations will be segmented from the light microscopy images. This will open an additional fluorescent channel for analysis. Further, implementing cell tracking algorithms will allow the observation of the development of sub-populations of cells. Following cells across space and time will add two new dimensions that can not be observed with traditional flow cytometry technologies.

5.2 ANTIOXIDANT CAPACITY: A NEW ADDITION TO STEMNESS?

Recent literature developments highlight the use of a new term "stemness" to describe the properties that define a stem cell (Dernbach et al., 2004; Ramalho-Santos et al., 2002). These include upregulation of genes responsible for self-renewal and cell fate. Perhaps an important unconsidered stem cell property is its antioxidant capacity and corresponding resistance to stress. This seems logical. An area of injury is a hostile environment for a cell with low levels of oxygen following ischemia or vessel damage followed by high levels of oxidative stress and inflammation after reperfusion. The success of a cell population to regenerate tissue would be dependent on the ability to function in this noxious environment. Studies presented here add important evidence to a growing body of literature about eth importance of a resistance to stress in stem and progenitor cell populations (Dernbach et al., 2004; Evens et al., 2004; He et al., 2004; Ramalho-Santos et al., 2002).

5.3 ANTIOXIDANT CAPACITY: IMPLICATIONS IN MDSC DEVELOPMENT

The important role of antioxidant capacity in the regenerative capacity of MDSCs also raises interesting questions regarding the developmental role of MDSCs. MDSCs are resistant to oxidative stress and myoblasts are impaired by oxidative stress, especially in their ability to fuse to form myotubes. As outlined in figure 4, MDSCs are believed to be a progenitor population of satellite cells and myoblasts because of the low levels of expression of myogenic markers. Further, it has been proposed that MDSC, satellite cell, and myoblast differentiation are related in a linear pattern. In this case, MDSCs differentiate into myofibers in a series of progressions to satellite cells and then myoblasts before fusing to form myofibers. This has two implications. First, there are two sources of oxidative stress: pre-transplantation and post-transplantation. If the majority of oxidative induced damage occurs prior to transplantation in a short time period, then this linear relationship between MDSCs and myoblasts is still plausible. Second, if oxidative stress plays a major role in the post-transplantation environment, then the relationship can become more complicated. If the levels of oxidative stress and ensuring inflammation persist over an extended period of time, then this suggests MDSC may have an alternative pathway to fuse and restore dystrophin-positive myofibers. Under a continuous level of oxidative stress and inflammation, if MDSCs differentiated into myoblasts, then these transplanted cells would be susceptible to oxidative stress as well, and the regenerative advantage of MDSCs as compared to myoblasts would be lost. This type of sink would be avoided if the levels of oxidative stress and inflammation occurred over a shorter time period in which MDSCs outlasted this stress and then differentiated into satellite cells. This would be similar to a time delayed response of MDSC to differentiation. These different scenarios are outlined in figure 21.

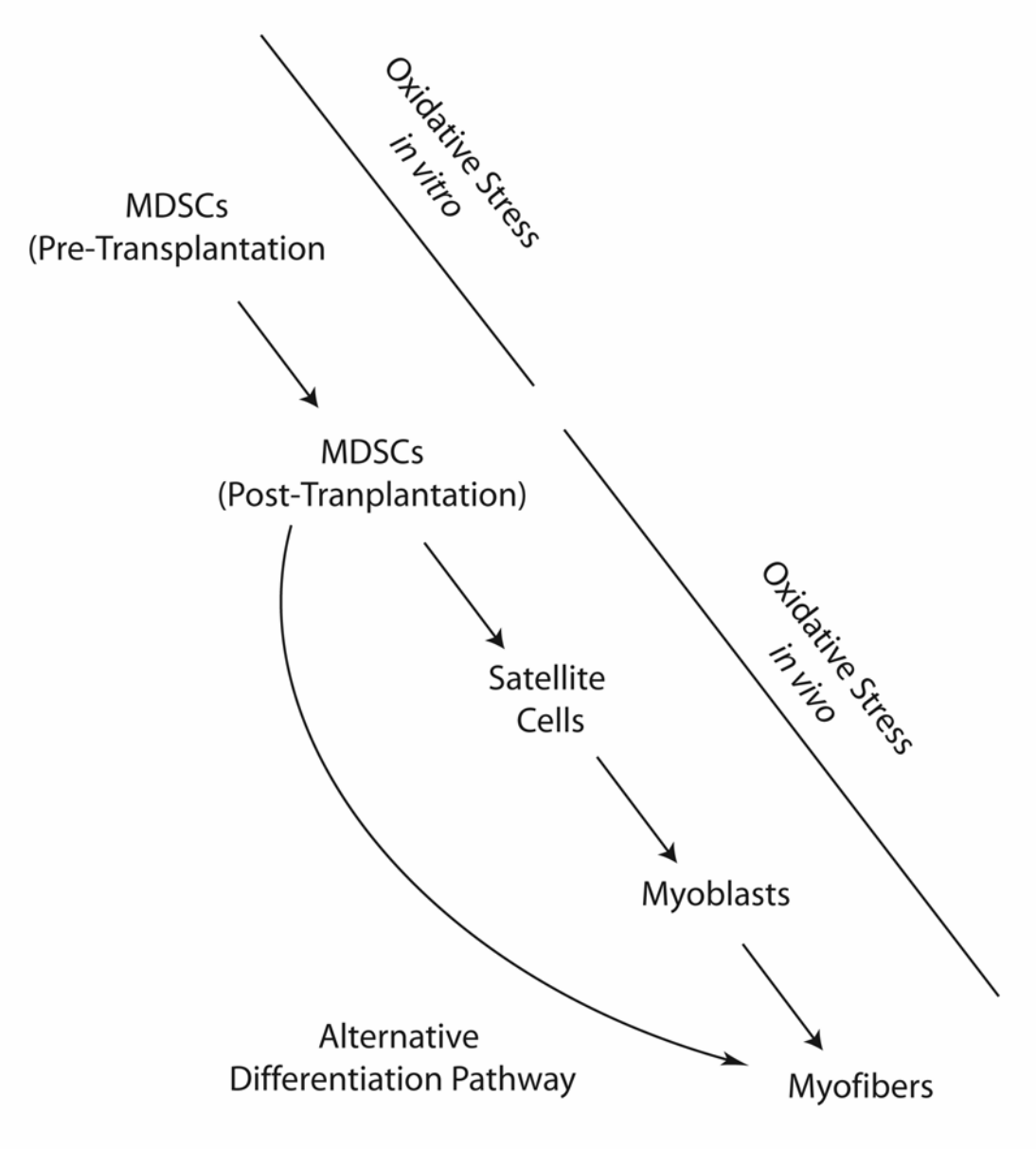

Figure 21: Possible Differentiation Pathways for MDSCs
MDSCs are believed to differentiate towards myofibers in a linear progression through satellite cells and myoblasts. This series, step-wise development is only possible if oxidative stress only plays a major role in the pre-transplantation environment during harvesting and handling of the cells or if MDSC differentiation is delayed until after oxidative stress and inflammation subsides *in vivo*. If MDSC differentiated into myoblasts in an environment of oxidative stress, then any regenerative advantage of the MDSCs as compared to myoblasts would be lost. Another possibility is that MDSCs differentiate into myofibers via an alternative pathway.

5.4 IMPLICATIONS FOR CELL THERAPIES

An important possible contribution of this work is in the area of cell therapies in regenerative medicine. A challenge in cell transplantation is the large variation in regenerative capacity of different cell populations across different isolations. Currently, it is impossible to predict the regenerative capacity of a cell population until after transplantation. This is unsuitable if these therapies will successfully be used in the clinic. Rapid assays need to be designed that can test the regenerative capacity of a cell population *in vitro* or directly after isolation prior to transplantation. These studies suggest that a cell's antioxidant phenotype may possess the potential to select populations of cells prior to transplantation to optimize tissue regeneration. Further, enhancing a cell population's antioxidant capacity may increase its regenerative capacity after transplantation *in vivo*.

BIBLIOGRAPHY

2005. Long-term self-renewal of postnatal muscle-derived stem cells. *Mol Biol Cell.* 16:3323-33. Epub 2005 May 4.

Ambrosio, G., and I. Tritto. 1999. Reperfusion injury: experimental evidence and clinical implications. *Am Heart J*. 138:S69-75.

Arahata, K., S. Ishiura, T. Ishiguro, T. Tsukahara, Y. Suhara, C. Eguchi, T. Ishihara, I. Nonaka, E. Ozawa, and H. Sugita. 1988. Immunostaining of skeletal and cardiac muscle surface membrane with antibody against Duchenne muscular dystrophy peptide. *Nature*. 333:861-3.

Bahnson, A., C. Athanassiou, D. Koebler, L. Qian, T. Shun, D. Shields, H. Yu, H. Wang, J. Goff, T. Cheng, R. Houck, and L. Cowsert. 2005. Automated measurement of cell motility and proliferation. *BMC Cell Biol*. 6:19.

Baroffio, A., M. Hamann, L. Bernheim, M.L. Bochaton-Piallat, G. Gabbiani, and C.R. Bader. 1996. Identification of self-renewing myoblasts in the progeny of single human muscle satellite cells. *Differentiation*. 60:47-57.

Beauchamp, J.R., L. Heslop, D.S. Yu, S. Tajbakhsh, R.G. Kelly, A. Wernig, M.E. Buckingham, T.A. Partridge, and P.S. Zammit. 2000. Expression of CD34 and Myf5 defines the majority of quiescent adult skeletal muscle satellite cells. *J Cell Biol*. 151:1221-34.

Beauchamp, J.R., J.E. Morgan, C.N. Pagel, and T.A. Partridge. 1994. Quantitative studies of efficacy of myoblast transplantation. *Muscle Nerve*. 18 (Suppl):261.

Beauchamp, J.R., J.E. Morgan, C.N. Pagel, and T.A. Partridge. 1999. Dynamics of myoblast transplantation reveal a discrete minority of precursors with stem cell-like properties as the myogenic source. *J Cell Biol*. 144:1113-22.

Bertera, S., M.L. Crawford, A.M. Alexander, G.D. Papworth, S.C. Watkins, P.D. Robbins, and M. Trucco. 2003. Gene transfer of manganese superoxide dismutase extends islet graft function in a mouse model of autoimmune diabetes. *Diabetes*. 52:387-93.

Bischoff, R. 1997. Chemotaxis of skeletal muscle satellite cells. *Dev Dyn*. 208:505-15.

Bittner, R.E., B. Streubel, S. Shorny, G. Schaden, T. Voit, and H. Hoger. 1994. Coisogenic all-plus-one immunization: a model for identifying missing proteins in null-mutant conditions. Antibodies to dystrophin in mdx mouse after transplantation of muscle from normal coisogenic donor. *Neuropediatrics*. 25:176-82.

Blackwell, T.S., J.W. Christman, T. Hagan, P. Price, T. Edens, P.E. Morris, S.N. Wolff, S.A. Goodman, and B.W. Christman. 2000. Oxidative stress and NF-kappaB activation: correlation in patients following allogeneic bone marrow transplantation. *Antioxid Redox Signal*. 2:93-102.

Bloch, K., and P. Vardi. 2005. Toxin-based selection of insulin-producing cells with improved defense properties for islet cell transplantation. *Diabetes Metab Res Rev*.

Bonilla, E., C.E. Samitt, A.F. Miranda, A.P. Hays, G. Salviati, S. DiMauro, L.M. Kunkel, E.P. Hoffman, and L.P. Rowland. 1988. Duchenne muscular dystrophy: deficiency of dystrophin at the muscle cell surface. *Cell*. 54:447-52.

Bosch, P., D. Musgrave, S. Ghivizzani, C. Latterman, C.S. Day, and J. Huard. 2000. The efficiency of muscle-derived cell-mediated bone formation. *Cell Transplant*. 9:463-70.

Bottino, R., A.N. Balamurugan, S. Bertera, M. Pietropaolo, M. Trucco, and J.D. Piganelli. 2002. Preservation of human islet cell functional mass by anti-oxidative action of a novel SOD mimic compound. *Diabetes*. 51:2561-7.

Bottino, R., A.N. Balamurugan, H. Tse, C. Thirunavukkarasu, X. Ge, J. Profozich, M. Milton, A. Ziegenfuss, M. Trucco, and J.D. Piganelli. 2004. Response of human islets to isolation stress and the effect of antioxidant treatment. *Diabetes*. 53:2559-68.

Boulanger, A., I. Asselin, R. Roy, and J.P. Tremblay. 1997. Role of non-major histocompatibility complex antigens in the rejection of transplanted myoblasts. *Transplantation*. 63:893-9.

Cao, B., B. Zheng, R.J. Jankowski, S. Kimura, M. Ikezawa, B. Deasy, J. Cummins, M. Epperly, Z. Qu-Petersen, and J. Huard. 2003. Muscle stem cells differentiate into haematopoietic lineages but retain myogenic potential. *Nat Cell Biol*. 5:640-6.

Carden, D.L., and D.N. Granger. 2000. Pathophysiology of ischaemia-reperfusion injury. *J Pathol*. 190:255-66.

Caron, N.J., I. Asselin, G. Morel, and J.P. Tremblay. 1999. Increased myogenic potential and fusion of matrilysin-expressing myoblasts transplanted in mice. *Cell Transplant*. 8:465-76.

Cornelison, D.D., and B.J. Wold. 1997. Single-cell analysis of regulatory gene expression in quiescent and activated mouse skeletal muscle satellite cells. *Dev Biol*. 191:270-83.

Dai, Y., M. Roman, R.K. Naviaux, and I.M. Verma. 1992. Gene therapy via primary myoblasts: long-term expression of factor IX protein following transplantation in vivo. *Proc Natl Acad Sci U S A*. 89:10892-5.

Deasy, B.M., B.M. Gharaibeh, J.B. Pollett, M.M. Jones, M.A. Lucas, Y. Kanda, and J. Huard. 2005. Long-term self-renewal of postnatal muscle-derived stem cells. *Mol Biol Cell*. 16:3323-33.

Deasy, B.M., R.J. Jankowski, and J. Huard. 2001. Muscle-derived stem cells: characterization and potential for cell-mediated therapy. *Blood Cells Mol Dis*. 27:924-33.

Deasy, B.M., R.J. Jankowski, T.R. Payne, B. Cao, J.P. Goff, J.S. Greenberger, and J. Huard. 2003. Modeling stem cell population growth: incorporating terms for proliferative heterogeneity. *Stem Cells*. 21:536-45.

Deasy, B.M., Z. Qu-Peterson, J.S. Greenberger, and J. Huard. 2002. Mechanisms of muscle stem cell expansion with cytokines. *Stem Cells*. 20:50-60.

Dernbach, E., C. Urbich, R.P. Brandes, W.K. Hofmann, A.M. Zeiher, and S. Dimmeler. 2004. Antioxidative stress-associated genes in circulating progenitor cells: evidence for enhanced resistance against oxidative stress. *Blood*. 104:3591-7.

Dhalla, N.S., L. Golfman, S. Takeda, N. Takeda, and M. Nagano. 1999. Evidence for the role of oxidative stress in acute ischemic heart disease: a brief review. *Can J Cardiol*. 15:587-93.

El Fahime, E., Y. Torrente, N.J. Caron, M.D. Bresolin, and J.P. Tremblay. 2000. In vivo migration of transplanted myoblasts requires matrix metalloproteinase activity. *Exp Cell Res*. 258:279-87.

Ervasti, J.M., and K.P. Campbell. 1991. Membrane organization of the dystrophin-glycoprotein complex. *Cell*. 66:1121-31.

Evens, A.M., J. Mehta, and L.I. Gordon. 2004. Rust and corrosion in hematopoietic stem cell transplantation: the problem of iron and oxidative stress. *Bone Marrow Transplant*. 34:561-71.

Fan, Y., M. Maley, M. Beilharz, and M. Grounds. 1996. Rapid death of injected myoblasts in myoblast transfer therapy. *Muscle Nerve*. 19:853-60.

Ferrer, A., K.E. Wells, and D.J. Wells. 2000. Immune responses to dystropin: implications for gene therapy of Duchenne muscular dystrophy. *Gene Ther*. 7:1439-46.

Goldring, K., T. Partridge, and D. Watt. 2002. Muscle stem cells. *J Pathol*. 197:457-67.

Gross, J.G., and J.E. Morgan. 1999. Muscle precursor cells injected into irradiated mdx mouse muscle persist after serial injury. *Muscle Nerve*. 22:174-85.

Grounds, M.D. 1996. Commentary on the present state of knowledge for myoblast transfer therapy. *Cell Transplant*. 5:431-3.

Grounds, M.D., and J.K. McGeachie. 1987. A model of myogenesis in vivo, derived from detailed autoradiographic studies of regenerating skeletal muscle, challenges the concept of quantal mitosis. *Cell Tissue Res*. 250:563-9.

Guerette, B., I. Asselin, D. Skuk, M. Entman, and J.P. Tremblay. 1997a. Control of inflammatory damage by anti-LFA-1: increase success of myoblast transplantation. *Cell Transplant*. 6:101-7.

Guerette, B., I. Asselin, J.T. Vilquin, R. Roy, and J.P. Tremblay. 1995. Lymphocyte infiltration following allo- and xenomyoblast transplantation in mdx mice. *Muscle Nerve*. 18:39-51.

Guerette, B., D. Skuk, F. Celestin, C. Huard, F. Tardif, I. Asselin, B. Roy, M. Goulet, R. Roy, M. Entman, and J.P. Tremblay. 1997b. Prevention by anti-LFA-1 of acute myoblast death following transplantation. *J Immunol*. 159:2522-31.

Gussoni, E., H.M. Blau, and L.M. Kunkel. 1997. The fate of individual myoblasts after transplantation into muscles of DMD patients. *Nat Med*. 3:970-7.

Gussoni, E., G.K. Pavlath, A.M. Lanctot, K.R. Sharma, R.G. Miller, L. Steinman, and H.M. Blau. 1992. Normal dystrophin transcripts detected in Duchenne muscular dystrophy patients after myoblast transplantation. *Nature*. 356:435-8.

Gussoni, E., Y. Soneoka, C.D. Strickland, E.A. Buzney, M.K. Khan, A.F. Flint, L.M. Kunkel, and R.C. Mulligan. 1999. Dystrophin expression in the mdx mouse restored by stem cell transplantation. *Nature*. 401:390-4.

Gute, D.C., T. Ishida, K. Yarimizu, and R.J. Korthuis. 1998. Inflammatory responses to ischemia and reperfusion in skeletal muscle. *Mol Cell Biochem*. 179:169-87.

He, T., T.E. Peterson, E.L. Holmuhamedov, A. Terzic, N.M. Caplice, L.W. Oberley, and Z.S. Katusic. 2004. Human endothelial progenitor cells tolerate oxidative stress due to intrinsically high expression of manganese superoxide dismutase. *Arterioscler Thromb Vasc Biol*. 24:2021-7.

Hempel, S.L., G.R. Buettner, Y.Q. O'Malley, D.A. Wessels, and D.M. Flaherty. 1999. Dihydrofluorescein diacetate is superior for detecting intracellular oxidants: comparison with 2',7'-dichlorodihydrofluorescein diacetate, 5(and 6)-carboxy-2',7'-dichlorodihydrofluorescein diacetate, and dihydrorhodamine 123. *Free Radic Biol Med*. 27:146-59.

Heslop, L., J.E. Morgan, and T.A. Partridge. 2000. Evidence for a myogenic stem cell that is exhausted in dystrophic muscle. *J Cell Sci*. 113 (Pt 12):2299-308.

Hoffman, E.P., R.H. Brown, Jr., and L.M. Kunkel. 1987. Dystrophin: the protein product of the Duchenne muscular dystrophy locus. *Cell*. 51:919-28.

Huard, J., J.P. Bouchard, R. Roy, C. Labrecque, G. Dansereau, B. Lemieux, and J.P. Tremblay. 1991a. Myoblast transplantation produced dystrophin-positive muscle fibres in a 16-year-old patient with Duchenne muscular dystrophy. *Clin Sci (Lond)*. 81:287-8.

Huard, J., J.P. Bouchard, R. Roy, F. Malouin, G. Dansereau, C. Labrecque, N. Albert, C.L. Richards, B. Lemieux, and J.P. Tremblay. 1992a. Human myoblast transplantation: preliminary results of 4 cases. *Muscle Nerve*. 15:550-60.

Huard, J., B. Cao, and Z. Qu-Petersen. 2003. Muscle-derived stem cells: potential for muscle regeneration. *Birth Defects Res Part C Embryo Today*. 69:230-7.

Huard, J., C. Labrecque, G. Dansereau, L. Robitaille, and J.P. Tremblay. 1991b. Dystrophin expression in myotubes formed by the fusion of normal and dystrophic myoblasts. *Muscle Nerve*. 14:178-82.

Huard, J., R. Roy, J.P. Bouchard, F. Malouin, C.L. Richards, and J.P. Tremblay. 1992b. Human myoblast transplantation between immunohistocompatible donors and recipients produces immune reactions. *Transplant Proc*. 24:3049-51.

Huard, J., R. Roy, B. Guerette, S. Verreault, G. Tremblay, and J.P. Tremblay. 1994a. Human myoblast transplantation in immunodeficient and immunosuppressed mice: evidence of rejection. *Muscle Nerve*. 17:224-34.

Huard, J., S. Verreault, R. Roy, M. Tremblay, and J.P. Tremblay. 1994b. High efficiency of muscle regeneration after human myoblast clone transplantation in SCID mice. *J Clin Invest*. 93:586-99.

Ibraghimov-Beskrovnaya, O., J.M. Ervasti, C.J. Leveille, C.A. Slaughter, S.W. Sernett, and K.P. Campbell. 1992. Primary structure of dystrophin-associated glycoproteins linking dystrophin to the extracellular matrix. *Nature*. 355:696-702.

Ito, H., P.L. Hallauer, K.E. Hastings, and J.P. Tremblay. 1998. Prior culture with concanavalin A increases intramuscular migration of transplanted myoblast. *Muscle Nerve*. 21:291-7.

Jackson, K.A., T. Mi, and M.A. Goodell. 1999. Hematopoietic potential of stem cells isolated from murine skeletal muscle. *Proc Natl Acad Sci U S A*. 96:14482-6.

Jankowski, R.J., B.M. Deasy, B. Cao, C. Gates, and J. Huard. 2002a. The role of CD34 expression and cellular fusion in the regeneration capacity of myogenic progenitor cells. *J Cell Sci*. 115:4361-4374.

Jankowski, R.J., B.M. Deasy, and J. Huard. 2002b. Muscle-derived stem cells. *Gene Ther*. 9:642-7.

Jankowski, R.J., C. Haluszczak, M. Trucco, and J. Huard. 2001. Flow cytometric characterization of myogenic cell populations obtained via the preplate technique: potential for rapid isolation of muscle-derived stem cells. *Hum Gene Ther*. 12:619-28.

Jankowski, R.J., and J. Huard. 2004. Establishing reliable criteria for isolating myogenic cell fractions with stem cell properties and enhanced regenerative capacity. *Blood Cells Mol Dis*. 32:24-33.

Karpati, G., D. Ajdukovic, D. Arnold, R.B. Gledhill, R. Guttmann, P. Holland, P.A. Koch, E. Shoubridge, D. Spence, M. Vanasse, and et al. 1993. Myoblast transfer in Duchenne muscular dystrophy. *Ann Neurol*. 34:8-17.

Karpati, G., Y. Pouliot, E. Zubrzycka-Gaarn, S. Carpenter, P.N. Ray, R.G. Worton, and P. Holland. 1989. Dystrophin is expressed in mdx skeletal muscle fibers after normal myoblast implantation. *Am J Pathol*. 135:27-32.

Kimura, S., M. Ikezawa, R. Pruchnic, L. Balkir, Z. Qu, J. Lowenstein, S. Takeda, C. Gates, B. Cao, T. Miike, and J. Huard. 2000. Persistent gene transfer to skeletal muscle mediated by stably transfected early myogenic progenitor cells. *Basic Appl Myol*. 10:237-48.

Kinoshita, I., J.T. Vilquin, B. Guerette, I. Asselin, R. Roy, and J.P. Tremblay. 1994. Very efficient myoblast allotransplantation in mice under FK506 immunosuppression. *Muscle Nerve*. 17:1407-15.

Labrecque, C., R. Roy, and J.P. Tremblay. 1992. Immune reactions after myoblast transplantation in mouse muscles. *Transplant Proc*. 24:2889-92.

Law, P.K., T.E. Bertorini, T.G. Goodwin, M. Chen, Q.W. Fang, H.J. Li, D.S. Kirby, J.A. Florendo, H.G. Herrod, and G.S. Golden. 1990. Dystrophin production induced by myoblast transfer therapy in Duchenne muscular dystrophy. *Lancet*. 336:114-5.

Law, P.K., T.G. Goodwin, and M.G. Wang. 1988. Normal myoblast injections provide genetic treatment for murine dystrophy. *Muscle Nerve*. 11:525-33.

Lee, J.Y., Z. Qu-Petersen, B. Cao, S. Kimura, R. Jankowski, J. Cummins, A. Usas, C. Gates, P. Robbins, A. Wernig, and J. Huard. 2000. Clonal isolation of muscle-derived cells capable of enhancing muscle regeneration and bone healing. *J Cell Biol*. 150:1085-100.

Lochmuller, H., B.J. Petrof, G. Pari, N. Larochelle, V. Dodelet, Q. Wang, C. Allen, S. Prescott, B. Massie, J. Nalbantoglu, and G. Karpati. 1996. Transient immunosuppression by FK506 permits a sustained high-level dystrophin expression after adenovirus-mediated dystrophin minigene transfer to skeletal muscles of adult dystrophic (mdx) mice. *Gene Ther*. 3:706-16.

Mammolenti, M., S. Gajavelli, P. Tsoulfas, and R. Levy. 2004. Absence of major histocompatibility complex class I on neural stem cells does not permit natural killer cell killing and prevents recognition by alloreactive cytotoxic T lymphocytes in vitro. *Stem Cells*. 22:1101-10.

Matsumura, K., and K.P. Campbell. 1994. Dystrophin-glycoprotein complex: its role in the molecular pathogenesis of muscular dystrophies. *Muscle Nerve*. 17:2-15.

Matsumura, K., J.M. Ervasti, K. Ohlendieck, S.D. Kahl, and K.P. Campbell. 1992. Association of dystrophin-related protein with dystrophin-associated proteins in mdx mouse muscle. *Nature*. 360:588-91.

McGeachie, J.K., and M.D. Grounds. 1987. Initiation and duration of muscle precursor replication after mild and severe injury to skeletal muscle of mice. An autoradiographic study. *Cell Tissue Res*. 248:125-30.

Menasche, P. 2004. Skeletal myoblast transplantation for cardiac repair. *Expert Rev Cardiovasc Ther*. 2:21-8.

Mendell, J.R., J.T. Kissel, A.A. Amato, W. King, L. Signore, T.W. Prior, Z. Sahenk, S. Benson, P.E. McAndrew, R. Rice, and et al. 1995. Myoblast transfer in the treatment of Duchenne's muscular dystrophy. *N Engl J Med*. 333:832-8.

Menke, A., and H. Jockusch. 1991. Decreased osmotic stability of dystrophin-less muscle cells from the mdx mouse. *Nature*. 349:69-71.

Miranda, A.F., E. Bonilla, G. Martucci, C.T. Moraes, A.P. Hays, and S. Dimauro. 1988. Immunocytochemical study of dystrophin in muscle cultures from patients with Duchenne muscular dystrophy and unaffected control patients. *Am J Pathol*. 132:410-6.

Molnar, G., M.L. Ho, and N.A. Schroedl. 1996. Evidence for multiple satellite cell populations and a non-myogenic cell type that is regulated differently in regenerating and growing skeletal muscle. *Tissue Cell*. 28:547-56.

Morgan, J.E., E.P. Hoffman, and T.A. Partridge. 1990. Normal myogenic cells from newborn mice restore normal histology to degenerating muscles of the mdx mouse. *J Cell Biol*. 111:2437-49.

Morgan, J.E., C.N. Pagel, T. Sherratt, and T.A. Partridge. 1993. Long-term persistence and migration of myogenic cells injected into pre-irradiated muscles of mdx mice. *J Neurol Sci*. 115:191-200.

Musgrave, D.S., P. Bosch, J.Y. Lee, D. Pelinkovic, S.C. Ghivizzani, J. Whalen, C. Niyibizi, and J. Huard. 2000. Ex vivo gene therapy to produce bone using different cell types. *Clin Orthop*:290-305.

Neumann, B., M. Held, U. Liebel, H. Erfle, P. Rogers, R. Pepperkok, and J. Ellenberg. 2006. High-throughput RNAi screening by time-lapse imaging of live human cells. *Nat Methods*. 3:385-90.

Ohtsuka, Y., K. Udaka, Y. Yamashiro, H. Yagita, and K. Okumura. 1998. Dystrophin acts as a transplantation rejection antigen in dystrophin-deficient mice: implication for gene therapy. *J Immunol*. 160:4635-40.

Olguin, H.C., and B.B. Olwin. 2004. Pax-7 up-regulation inhibits myogenesis and cell cycle progression in satellite cells: a potential mechanism for self-renewal. *Dev Biol*. 275:375-88.

Oshima, H., T.R. Payne, K.L. Urish, T. Sakai, Y. Ling, B. Gharaibeh, M. Tobita, B.B. Keller, J. Cummins, and J. Huard. 2005. Differential Myocardial Infarct Repair with Muscle Stem Cells Compared to Myoblasts. *Mol Ther*. In Press.

Otsu, N. 1979. A Threshold Selection Method From Gray Level Histograms. *IEEE Transactions on Systems, Man ,and Cybernetics*. SMC-9:62-66.

Oustanina, S., G. Hause, and T. Braun. 2004. Pax7 directs postnatal renewal and propagation of myogenic satellite cells but not their specification. *Embo J*. 23:3430-9.

Ozawa, E., M. Yoshida, A. Suzuki, Y. Mizuno, Y. Hagiwara, and S. Noguchi. 1995. Dystrophin-associated proteins in muscular dystrophy. *Hum Mol Genet*. 4 Spec No:1711-6.

Partridge, T.A., J.E. Morgan, G.R. Coulton, E.P. Hoffman, and L.M. Kunkel. 1989. Conversion of mdx myofibres from dystrophin-negative to -positive by injection of normal myoblasts. *Nature*. 337:176-9.

Perlman, Z.E., M.D. Slack, Y. Feng, T.J. Mitchison, L.F. Wu, and S.J. Altschuler. 2004. Multidimensional drug profiling by automated microscopy. *Science*. 306:1194-8.

Pikaz, A., and A. Averbuch. 1996. Digital Image thresholding Based on Topological Stable-State. *Pattern Recognition*. 29:829-843.

Plummer, J.L., B.R. Smith, H. Sies, and J.R. Bend. 1981. Chemical depletion of glutathione in vivo. *Methods Enzymol*. 77:50-9.

Qu, Z., L. Balkir, J.C. van Deutekom, P.D. Robbins, R. Pruchnic, and J. Huard. 1998. Development of approaches to improve cell survival in myoblast transfer therapy. *J Cell Biol*. 142:1257-67.

Qu, Z., and J. Huard. 2000. Matching host muscle and donor myoblasts for myosin heavy chain improves myoblast transfer therapy. *Gene Ther*. 7:428-37.

Quinlan, J.G., S.P. Lyden, D.M. Cambier, S.R. Johnson, S.E. Michaels, and D.L. Denman. 1995. Radiation inhibition of mdx mouse muscle regeneration: dose and age factors. *Muscle Nerve*. 18:201-6.

Qu-Petersen, Z., B. Deasy, R. Jankowski, M. Ikezawa, J. Cummins, R. Pruchnic, J. Mytinger, B. Cao, C. Gates, A. Wernig, and J. Huard. 2002. Identification of a novel population of muscle stem cells in mice: potential for muscle regeneration. *J Cell Biol*. 157:851-64.

Ramalho-Santos, M., S. Yoon, Y. Matsuzaki, R.C. Mulligan, and D.A. Melton. 2002. "Stemness": transcriptional profiling of embryonic and adult stem cells. *Science*. 298:597-600.

Rando, T.A., and H.M. Blau. 1994. Primary mouse myoblast purification, characterization, and transplantation for cell-mediated gene therapy. *J Cell Biol*. 125:1275-87.

Richler, C., and D. Yaffe. 1970. The in vitro cultivation and differentiation capacities of myogenic cell lines. *Dev Biol*. 23:1-22.

Sampaolesi, M., Y. Torrente, A. Innocenzi, R. Tonlorenzi, G. D'Antona, M.A. Pellegrino, R. Barresi, N. Bresolin, M.G. De Angelis, K.P. Campbell, R. Bottinelli, and G. Cossu. 2003. Cell therapy of alpha-sarcoglycan null dystrophic mice through intra-arterial delivery of mesoangioblasts. *Science*. 301:487-92.

Satoh, A., J. Huard, C. Labrecque, and J.P. Tremblay. 1993. Use of fluorescent latex microspheres (FLMs) to follow the fate of transplanted myoblasts. *J Histochem Cytochem*. 41:1579-82.

Schultz, E. 1996. Satellite cell proliferative compartments in growing skeletal muscles. *Dev Biol*. 175:84-94.

Seale, P., and M.A. Rudnicki. 2000. A new look at the origin, function, and "stem-cell" status of muscle satellite cells. *Dev Biol*. 218:115-24.

Seale, P., L.A. Sabourin, A. Girgis-Gabardo, A. Mansouri, P. Gruss, and M.A. Rudnicki. 2000. Pax7 is required for the specification of myogenic satellite cells. *Cell*. 102:777-86.

Seamer, L.C., C.B. Bagwell, L. Barden, D. Redelman, G.C. Salzman, J.C. Wood, and R.F. Murphy. 1997. Proposed new data file standard for flow cytometry, version FCS 3.0. *Cytometry*. 28:118-22.

Shen, H.C., H. Peng, A. Usas, B. Gearhart, J. Cummins, F.H. Fu, and J. Huard. 2004a. Ex vivo gene therapy-induced endochondral bone formation: comparison of muscle-derived stem cells and different subpopulations of primary muscle-derived cells. *Bone*. 34:982-92.

Shen, H.C., H. Peng, A. Usas, B. Gearhart, F.H. Fu, and J. Huard. 2004b. Structural and functional healing of critical-size segmental bone defects by transduced muscle-derived cells expressing BMP4. *J Gene Med*. 6:984-91.

Sigal, A., R. Milo, A. Cohen, N. Geva-Zatorsky, Y. Klein, I. Alaluf, N. Swerdlin, N. Perzov, T. Danon, Y. Liron, T. Raveh, A.E. Carpenter, G. Lahav, and U. Alon. 2006. Dynamic proteomics in individual human cells uncovers widespread cell-cycle dependence of nuclear proteins. *Nat Methods*. 3:525-31.

Smythe, G.M., Y. Fan, and M.D. Grounds. 2000. Enhanced migration and fusion of donor myoblasts in dystrophic and normal host muscle. *Muscle Nerve*. 23:560-74.

Suzuki, K., B. Murtuza, J.R. Beauchamp, R.T. Smolenski, A. Varela-Carver, S. Fukushima, S.R. Coppen, T.A. Partridge, and M.H. Yacoub. 2004. Dynamics and mediators of acute graft attrition after myoblast transplantation to the heart. *Faseb J*. 18:1153-5.

Suzuki, K., R.T. Smolenski, J. Jayakumar, B. Murtuza, N.J. Brand, and M.H. Yacoub. 2000. Heat shock treatment enhances graft cell survival in skeletal myoblast transplantation to the heart. *Circulation*. 102:III216-21.

Takuma, S., K. Suehiro, C. Cardinale, T. Hozumi, H. Yano, J. Shimizu, S. Mullis-Jansson, R. Sciacca, J. Wang, D. Burkhoff, M.R. Di Tullio, and S. Homma. 2001. Anesthetic inhibition in ischemic and nonischemic murine heart: comparison with conscious echocardiographic approach. *Am J Physiol Heart Circ Physiol*. 280:H2364-70.

Taylor, D.A., B.Z. Atkins, P. Hungspreugs, T.R. Jones, M.C. Reedy, K.A. Hutcheson, D.D. Glower, and W.E. Kraus. 1998. Regenerating functional myocardium: improved performance after skeletal myoblast transplantation. *Nat Med*. 4:929-33.

Team, R.D.C. 2006. R: A Language and Environment for Statistical Computing, Vienna.

Torrente, Y., G. Camirand, F. Pisati, M. Belicchi, B. Rossi, F. Colombo, M. El Fahime, N.J. Caron, A.C. Issekutz, G. Constantin, J.P. Tremblay, and N. Bresolin. 2003. Identification of a putative pathway for the muscle homing of stem cells in a muscular dystrophy model. *J Cell Biol*. 162:511-20.

Torrente, Y., E. El Fahime, N.J. Caron, N. Bresolin, and J.P. Tremblay. 2000. Intramuscular migration of myoblasts transplanted after muscle pretreatment with metalloproteinases. *Cell Transplant*. 9:539-49.

Torrente, Y., J.P. Tremblay, F. Pisati, M. Belicchi, B. Rossi, M. Sironi, F. Fortunato, M. El Fahime, M.G. D'Angelo, N.J. Caron, G. Constantin, D. Paulin, G. Scarlato, and N. Bresolin. 2001. Intraarterial injection of muscle-derived CD34(+)Sca-1(+) stem cells restores dystrophin in mdx mice. *J Cell Biol*. 152:335-48.

Tremblay, J.P., F. Malouin, R. Roy, J. Huard, J.P. Bouchard, A. Satoh, and C.L. Richards. 1993. Results of a triple blind clinical study of myoblast transplantations without immunosuppressive treatment in young boys with Duchenne muscular dystrophy. *Cell Transplant*. 2:99-112.

Urish, K.L., Y. Kanda, and J. Huard. 2005. Initial failure in myoblast transplantation therapy has led the way toward the isolation of muscle stem cells: Potential for tissue regeneration. *Curr Top Dev Biol*. 68:263-280.

Vilches, C., and P. Parham. 2002. KIR: diverse, rapidly evolving receptors of innate and adaptive immunity. *Annu Rev Immunol*. 20:217-51.

Vilquin, J.T., E. Wagner, I. Kinoshita, R. Roy, and J.P. Tremblay. 1995. Successful histocompatible myoblast transplantation in dystrophin-deficient mdx mouse despite the production of antibodies against dystrophin. *J Cell Biol*. 131:975-88.

Wakeford, S., D.J. Watt, and T.A. Partridge. 1991. X-irradiation improves mdx mouse muscle as a model of myofiber loss in DMD. *Muscle Nerve*. 14:42-50.

Watkins, S.C., E.P. Hoffman, H.S. Slayter, and L.M. Kunkel. 1988. Immunoelectron microscopic localization of dystrophin in myofibres. *Nature*. 333:863-6.

Watt, D.J., K. Lambert, J.E. Morgan, T.A. Partridge, and J.C. Sloper. 1982. Incorporation of donor muscle precursor cells into an area of muscle regeneration in the host mouse. *J Neurol Sci*. 57:319-31.

Watt, D.J., J.E. Morgan, and T.A. Partridge. 1984. Use of mononuclear precursor cells to insert allogeneic genes into growing mouse muscles. *Muscle Nerve*. 7:741-50.

Yoo, T.S., M.J. Ackerman, W.E. Lorensen, W. Schroeder, V. Chalana, S. Aylward, D. Metaxes, and R. Whitaker. 2002. Engineering and Algorithm Design for an Image Processing API: A Technical Report on ITK - The Insight Toolkit. IOS Press, Amsterdam. 586-592 pp.

Yoshida, N., S. Yoshida, K. Koishi, K. Masuda, and Y. Nabeshima. 1998. Cell heterogeneity upon myogenic differentiation: down-regulation of MyoD and Myf-5 generates 'reserve cells'. *J Cell Sci*. 111 (Pt 6):769-79.

Zammit, P., and J. Beauchamp. 2001. The skeletal muscle satellite cell: stem cell or son of stem cell? *Differentiation*. 68:193-204.

Zammit, P.S., J.P. Golding, Y. Nagata, V. Hudon, T.A. Partridge, and J.R. Beauchamp. 2004. Muscle satellite cells adopt divergent fates: a mechanism for self-renewal? *J Cell Biol*. 166:347-57.

Zhang, M., D. Methot, V. Poppa, Y. Fujio, K. Walsh, and C.E. Murry. 2001. Cardiomyocyte grafting for cardiac repair: graft cell death and anti-death strategies. *J Mol Cell Cardiol*. 33:907-21.

Zhao, Z.Q. 2004. Oxidative stress-elicited myocardial apoptosis during reperfusion. *Curr Opin Pharmacol*. 4:159-65.

Zubrzycka-Gaarn, E.E., D.E. Bulman, G. Karpati, A.H. Burghes, B. Belfall, H.J. Klamut, J. Talbot, R.S. Hodges, P.N. Ray, and R.G. Worton. 1988. The Duchenne muscular dystrophy gene product is localized in sarcolemma of human skeletal muscle. *Nature*. 333:466-9.